UQAC
Université du Québec
à Chicoutimi

Effets de la défoliation par la tordeuse des bourgeons de l'épinette sur la croissance et l'utilisation de l'eau chez l'épinette noire et le sapin baumier

par Caroline Rodrigues da Silva

Mémoire présenté à l'Université du Québec à Chicoutimi en vue de l'obtention du grade de Maîtrise ès sciences (M. Sc.) en Ressources Renouvelables

Québec, Canada

RÉSUMÉ

La défoliation causée par la tordeuse des bourgeons de l'épinette (*Choristoneura fumiferana*) est un facteur majeur de perturbation dans les forêts boréales. Le sapin baumier (*Abies balsamea*), son hôte principal, est généralement plus affecté que l'épinette noire (*Picea mariana*) avec une mortalité accrue. Ces infestations d'insectes réduisent la transpiration et la croissance des arbres, perturbent la dynamique de l'allocation des réserves et peuvent transformer les forêts de puits en sources de carbone. En 2021, la tordeuse a défolié environ 5 millions d'hectares, contribuant ainsi aux 15 953 011 hectares touchés par les insectes au Canada (4,34 % de la superficie forestière totale). Elle a également des conséquences directes sur le secteur forestier, car la mortalité des arbres et les pertes de croissance ont une incidence sur les estimations de coupe autorisée et l'approvisionnement en bois. La réduction de la croissance due à la défoliation peut être évaluée de façon continue en suivant la variation radiale du tronc à l'aide de dendromètres automatiques, qui enregistrent les contractions et les expansions réversibles liées à l'état hydrique et à la croissance des arbres. En séparant la croissance des signaux liés à l'eau, ces données capturent l'expansion radiale estivale et les relations hydriques des arbres, ainsi que la dynamique de la saison froide, notamment la déshydratation automnale, le gel hivernal et la réhydratation printanière. Nous avons développé des méthodes analytiques pour évaluer les effets de la tordeuse des bourgeons de l'épinette sur les cycles saisonniers de la transpiration des arbres et la variation radiale du tronc. Notre objectif était de suivre le flux de sève et la variation radiale du tronc chez l'épinette noire et le sapin baumier, afin de quantifier l'effet d'une épidémie sur leurs cycles saisonniers. Nous avons émis l'hypothèse que (i) une défoliation plus intense pendant la phase de transpiration et de croissance amplifie la baisse du flux de sève et de la variation radiale du tronc, avec des effets qui se prolongent aux phases suivantes, et (ii) qu'un déficit de pression de vapeur élevé (VPD) renforce cette réponse en cas de forte défoliation.

Les données ont été collectées sur huit arbres (quatre par espèce) dans le parc national des Monts-Valin (QC, Canada) entre 2017 et 2025. Des dendromètres à point ont été utilisés pour surveiller la variation radiale, calculer un index de croissance et quantifier les amplitudes de contraction ou d'expansion saisonnières. Des fluxmètres ont mesuré la densité du flux de sève et la transpiration du printemps à l'automne. Ces indices physiologiques ont été examinés parallèlement à la défoliation annuelle cumulative causée par la tordeuse des bourgeons de l'épinette et aux données climatiques *in situ*. À l'aide d'une approche mathematique, nous avons délimité cinq phases physiologiques récurrentes dans la variation radiale du tronc : déshydratation hivernale, état de gel, réhydratation printanière, transpiration et croissance, et fin de la transpiration et de la croissance.

Chez les deux espèces, les amplitudes radiales saisonnières du tronc ont généralement diminué avec l'augmentation de la défoliation cumulative, tandis que l'état de gel est resté relativement stable. La déshydratation hivernale est apparue comme une phase intégrative clé : l'amplitude mesurée en fin de saison de croissance (fin de la transpiration et de la croissance) était négativement corrélée à la déshydratation hivernale subséquente, autant chez l'épinette noire ($r = 0,77$) que le sapin baumier ($r = 0,81$). Par la suite une déshydratation hivernale plus forte était liée à une réhydratation printanière ($r = 0,82$) et une transpiration et une croissance ($r = 0,87$) ultérieures réduites, mais chez le sapin baumier uniquement. Le couplage entre l'utilisation de l'eau et la croissance différait également entre les espèces, car l'utilisation quotidienne moyenne de l'eau expliquait l'amplitude de la transpiration et de la croissance chez le sapin baumier ($R^2 = 0,64$; $p < 0,001$), mais pas chez l'épinette noire ($R^2 = 0,05$). Pour les deux espèces, l'utilisation de l'eau augmentait avec le VPD ($\hat{\beta} = 1,795$; $SE = 0,109$; $p < 0,001$), mais la réponse était moins sensible chez le sapin baumier que chez l'épinette noire (interaction VPD × espèce : $\hat{\beta} = -0,526$; $SE = 0,066$; $p < 0,001$). Au fil des ans, les effets de la tordeuse des bourgeons de l'épinette se sont prolongés au-delà de la période de défoliation, avec des effets résiduels qui ont persisté dans l'amplitude des phases et les années suivantes. Les réponses différaient entre les espèces, indiquant des stratégies hydrauliques contrastées : le sapin baumier présentait un couplage plus étroit entre la consommation d'eau et la croissance et une capacité moindre à amortir la perte des aiguilles sous défoliation, tandis que l'épinette noire affichait une régulation plus conservatrice qui atténuait la propagation interphasique du stress hydrique. Dans l'ensemble, l'approche présentée ici offre un moyen robuste de suivre la dynamique physiologique saisonnière et de quantifier la vulnérabilité et la résilience des conifères boréaux sous l'effet de la pression biotique et de la variabilité climatique.

Mots clés : défoliation causée par la tordeuse des bourgeons de l'épinette ; variation du rayon de la tige ; flux de sève ; épinette noire ; sapin baumier.

ABSTRACT

Defoliation caused by the spruce budworm (*Choristoneura fumiferana*) is a major factor of disturbance in boreal forests. Balsam fir (*Abies balsamea*), its main host, is generally more affected than black spruce (*Picea mariana*), with increased mortality. These insect infestations reduce tree transpiration and growth, disrupt the dynamics of reserve allocation, and can transform forests from carbon sinks into carbon sources. In 2021, the moth defoliated approximately 5 million hectares, contributing to the 15,953,011 hectares affected by insects in Canada (4.34% of the total forest area). It also has direct consequences for the forestry sector, as tree mortality and growth losses affect allowable cut estimates and wood supply. The reduction in growth due to defoliation can be assessed continuously by monitoring radial trunk variation using automatic dendrometers, which record reversible contractions and expansions related to tree water status and growth. By separating growth from water-related signals, these data capture summer radial expansion and tree water relations, as well as cold season dynamics, including fall dehydration, winter freezing, and spring rehydration. We developed analytical methods to assess the effects of spruce budworm on seasonal tree transpiration cycles and radial trunk variation. Our goal was to track sap flow and radial trunk variation in black spruce and balsam fir to quantify the effect of an outbreak on their seasonal cycles. We hypothesized that (i) more intense defoliation during the transpiration and growth phase amplifies the decline in sap flow and radial trunk variation, with effects that extend into subsequent phases, and that (ii) a high vapor pressure deficit (VPD) enhances this response in the event of heavy defoliation.

Data were collected on eight trees (four per species) in Monts-Valin National Park (QC, Canada) between 2017 and 2025. Point dendrometers were used to monitor radial variation, calculate a growth index, and quantify seasonal contraction or expansion amplitudes. Flow meters measured sap flow density and transpiration from spring to fall. These physiological indices were examined in conjunction with cumulative annual defoliation caused by spruce budworm and *in situ* climate data. Using an analytical approach, we identified five recurring physiological phases in trunk radial variation: winter dehydration, freezing state, spring rehydration, transpiration and growth, and end of transpiration and growth.

In both species, seasonal radial trunk growth generally decreased with increasing cumulative defoliation, while frost damage remained relatively stable. Winter dehydration emerged as a key integrative phase: the amplitude measured at the end of the growing season (end of transpiration and growth) was negatively correlated with subsequent winter dehydration in both black spruce ($r = 0.77$) and balsam fir ($r = 0.81$). Subsequently, greater winter dehydration was associated with spring rehydration ($r = 0.82$) and reduced subsequent transpiration and growth ($r = 0.87$), but only in balsam fir. The coupling between water use and growth also differed between species, as average daily water use explained the magnitude of transpiration and growth in balsam fir ($R^2 = 0.64$; $p < 0.001$), but not in black spruce ($R^2 = 0.05$). In both species, water use increased with VPD ($\hat{\beta} = 1.795$; SE = 0.109; $p < 0.001$), but the response was less sensitive in balsam fir than in black spruce (VPD × species interaction: $\hat{\beta} = -0.526$; SE = 0.066; $p < 0.001$). Over the years, the effects of spruce budworm extended beyond the defoliation period, with residual effects persisting in phase amplitude and subsequent years. Responses differed between species, indicating contrasting hydraulic strategies: balsam fir showed a closer coupling between water consumption and growth and a lower ability to buffer needle loss under defoliation, while black spruce exhibited more conservative regulation that mitigated interphase stress propagation. Overall, the approach presented here provides a robust means of tracking seasonal physiological dynamics and quantifying the vulnerability and resilience of boreal conifers under biotic pressure and climate variability.

Keywords: spruce budworm defoliation; stem radius variation; sap flow; black spruce; balsam fir.

TABLE DES MATIÈRES

LISTE DES TABLEAUX

LISTE DES FIGURES

DÉDICACE

À ma grand-mère Maria José Lisboa Rodrigues: à mesure que ce mémoire prenait son point final sur le papier, ta mémoire devenait éternité en moi.

REMERCIEMENTS

This master's degree came to an end thanks to the contribution of many people who sustained me throughout the journey, and, like Isaac Newton, who said he saw farther by standing on the shoulders of giants, today I want to name my giants.

Merci beaucoup, Annie Deslauriers, for this opportunity to enter another research area, for investing in me, and for allowing me to live such incredible experiences, not only in the academic world, but also in my personal life. For having trusted my potential, even when I questioned myself.

Muito obrigada, Mauro Brum, for guiding me with partnership, patience, friendship, and respect. For supporting and encouraging me from the beginning, sharing far beyond the advisor–advisee relationship, because the reality of a Brazilian immigrant from São Paulo, here in Chicoutimi, was and is challenging.

I thank the professors and students of the EcoTer laboratory for the studies and reflections we shared, as well as all the professionals and staff of the *Maîtrise en Ressources Renouvelables* program, who were essential to my professional and personal growth. Especially Germain Savard, *merci beaucoup* for each *mot du jour*, for celebrating with me my first *courriel* written in French, and for each *bonjour* accompanied by a beautiful smile. François Gionest, *merci* for all the help with data collection in Gaspard, for teaching me how the sensors work, and for giving me my first experience in the forest, here in Québec. And Catherine Tremblay, always present to answer my needs and my questions.

Many people passed through our laboratory, such as visiting researchers, exchange students, or graduate students, and you always added something positive to my life. To the people from other programs I met here and shared this journey with, my sincere thanks as well! Gian and Sara, *obrigada* for all the exchanges we had; I will keep your friendship with great affection. Rosario, *muchas gracias* for all the support, always with so much warmth and with the cutest Portuguese accent in the world!

To the girls Lais, Greta, Débora, Denise, Elizabeth, and Thanuri, who welcomed me and, little by little, integrated me not only into the University, but also into life, making us become a beautiful team. Thank you very much for sharing every glance, every smile, and tears - of joy and of insecurities - inside and outside UQAC! I also thank Franca and Junior for having welcomed me as parents here.

To Professor Fabrizio, for having welcomed and guided me so well during my internship, and to all colleagues at UNINA: *grazie mille*! *Merci beaucoup* à Valérie, for all the support during this period. Matteo, Sabrina, Mario, Giorgio, and Luisa, you were incredible hosts, because I loved getting to know a bit of Neapolitan culture through your eyes. *Grazie mille*!

Antonio and Joelita, you are the most incredible parents in the world. To you, all my love, respect, and gratitude. *Muito obrigada* for always encouraging me to study, to pursue my dreams, and for giving me support to achieve them. *Muito obrigada* for teaching me to dream, for every prayer, every video call, for celebrating each achievement with me, and for sharing moments of tears. You are my foundation and my reference, my greatest source of pride and inspiration. *Eu amo vocês*!

To my brothers, my first friends, *muito obrigada*. Christopher, since 2021 you invited me to come to Québec; I thank you for not giving up on this idea until I got here. You have always been a reference for me; it's no wonder we are so similar in some ways. In this journey as an international master's student, it is rare to be able to walk with family physically nearby, but I have you and now, Afsheen. *Obrigada* for being my family and my safe harbor here. Afsheen, you contributed greatly to my academic life, providing support, tips, and assistance, in addition to being family. Jefferson, you have always been my partner for outings, for dancing, for conversations, and for trips. I miss you very much and miss sharing life more closely. *Obrigada* for teaching me that life should be lived lightly, always taking the best from each phase. *Eu amo vocês, meus irmãos*!

Bianca, Daniel, and Brian, our friendship began at the start of academic life, when we crossed paths in the corridors of *Universidade Presbiteriana Mackenzie*. *Obrigada* for staying with me since then and for living yet another adventure. *Eu amo vocês*, bests!

Taís, Natalia, Marcos, and Leo, you are friends whom adult life gifted me and who sustained me from *Brasil* to Chicoutimi, through long video calls and endless messages. As one of the songs we like says: "*A amizade é tudo*".

To Professor Adilson de Morais, from *Universidade Presbiteriana Mackenzie*, and Professor Maria José Ferreira da Silva, from *Pontifícia Universidade Católica de São Paulo*, who guided me in my first master's degree in *Brasil* and became friends, my gratitude. You continue to be an inspiration.

To the Brazilian community that welcomed me here with open arms and makes me feel closer to home. As Lu says, *nós somos uma família*! You welcomed my brother and included me: *meu muito obrigada*.

AVANT-PROPOS

Ce mémoire a été structuré sous la forme d'un article scientifique et s'organise en plusieurs chapitres : Introduction, Chapitre 1 – Matériels et méthodes, Chapitre 2 – Résultats, Chapitre 3 – Discussion, et Conclusion.

Ce travail sera soumis sous forme d'article, rédigé en anglais à la revue *Environmental and Experimental Botany*, sous le titre « *Effects of defoliation by the spruce budworm on growth and water use in black spruce and balsam fir* ».

Les auteurs de ce travail sont Caroline Rodrigues da Silva[1*] ; Mauro Brum[2] ; et Annie Deslauriers[1].

Leurs affiliations sont les suivantes : [1] Laboratoire sur les écosystèmes terrestres boréaux, Département des Sciences Fondamentales, Université du Québec à Chicoutimi, Saguenay, QC, Canada ; et [2] Institute of Biological Sciences, *Universidade Federal do Pará*, Belém, PA, Brésil. L'auteure correspondante est Caroline Rodrigues da Silva (rdcaroline@etu.uqac.ca). En ce qui concerne les contributions des auteurs selon la taxonomie CRediT, la conceptualisation a été réalisée par CR, AD et MB ; la curation des données par CR ; l'analyse formelle par CR ; la recherche par CR et AD ; la méthodologie par CR, AD et MB ; la validation par CR, AD et MB ; la visualisation par CR ; la rédaction de la version originale par CR ; et la révision et l'édition du texte par AD et MB.

INTRODUCTION

BACKGROUND AND PROBLEM STATEMENT

Boreal forests are prominently located in Canada, representing about 9% of the world's forested area (FAO 2020), and the country hosts approximately 28% (552 million hectares) of the world's boreal zone (NRC 2024). This ecosystem occurs in high-latitude regions characterized by severe winters, with subzero temperatures lasting 6 to 8 months, and a short growing season (Burton *et al.* 2010). Boreal forests are marked by low tree-species diversity (Burton *et al.* 2010), notably conifers such as *Picea* (spruces) and *Abies* (firs). In Canadian forests, periodic insect outbreaks, alongside fires, represent the two primary annual natural disturbances (MacLean 2016). In Eastern North America's boreal forests, balsam fir and black spruce are predominantly affected by cyclic infestations of the eastern spruce budworm (SBW), with balsam fir serving as the primary host and black spruce as the secondary host (MacLean 1980; Régnière *et al.* 1989; Morin 1994; Nealis et Régnière 2004; Virgin et MacLean 2017; Balducci *et al.* 2021a). In 2023, 11.6 million hectares (ha) of Canada's forests, out of a total of 368,672,267 ha, were affected by insects (CFS 2025). From 2014 (about 3.6 million ha) to 2023 (approximately 5.9 million ha), the forest area disturbed by the eastern spruce budworm exhibited an overall increasing trend, despite marked interannual fluctuations, with peaks in 2020 (approximately 7.0 million ha) and 2022 (about 6.8 million ha) (NRC 2025). Throughout this period, Québec remained the most affected province. In 2024, the area defoliated by eastern spruce budworm in Québec reached 14,346,184 ha (MRNF 2025).

Spruce budworm defoliation [*Choristoneura fumiferana* (Clem.)] significantly alters ecosystem functioning in boreal forests. These infestations reduce transpiration and growth (Bouzidi *et al.* 2019; Balducci *et al.* 2020) affect carbon dynamics, and can shift forests from carbon sinks to carbon sources (Dymond *et al.* 2010; Liu *et al.* 2019). By decreasing photosynthesis and increasing organic matter decomposition, infestations may reduce carbon stocks by up to 3.4 TgC per year in Québec (Dymond *et al.* 2010). For the forest industry, mortality and reduced growth in these tree species affect estimates of annual allowable cut and wood production (Pothier *et al.* 2012).

The severity of growth reduction and mortality is closely linked to outbreak intensity and is influenced by factors such as population density, outbreak duration, feeding behavior, and host susceptibility (MacLean 2016). Spruce budworm typically consumes only a portion of the foliage, primarily the developing current-year needles, and can take years to kill a tree (Blais 1958; MacLean 2016). As a result, spruce budworm outbreaks can last from one to approximately 20 years, with moderate to severe annual impacts (MacLean 2016; Balducci *et al.* 2021a). Damage caused by spruce budworm typically become visible by June, corresponding to the peak feeding activity of the final larval instars (Bouzidi *et al.* 2019; Fortin *et al.* 2022). This damage is characterized by the destruction of vegetative buds, the extensive defoliation of current-year growth, and the presence of larvae dispersing or suspended from silk threads (Blais 1952; Koller et Leonard 1981; MacLean et Ostaff 1989; Bouzidi *et al.* 2019). Under high population densities, the forest canopy often develops a distinctive reddish-brown or scorched appearance by mid- to late June as partially consumed needles dry out and remain attached to branch tips by larval silk (MacLean et Ostaff 1989).

Historically, tree vitality and mortality have been studied predominantly through tree-ring analysis at the stand level, while individual tree-level physiological processes have remained less explored, except for of primary meristem phenology (i.e., leafing and budburst) and carbon reserves (Rossi et Bousquet 2014; Balducci *et al.* 2020). At the tree level, the physiological impact of defoliation on tree vitality and performance can also be studied using high temporal resolution time series of sap flow and stem radius variation (Steppe *et al.* 2006; Steppe *et al.* 2015b; Bouzidi *et al.* 2019; Balducci *et al.* 2020). The used of stem radius variation also provided information not only on stem growth but also on other processed such as autumn desiccation and spring stem rehydration (Turcotte *et al.* 2009). Nevertheless, these non-growth-related processes remain insufficiently investigated in trees affected by defoliation (Paixao *et al.* 2019). Sap flow measurements are essential for determining transpiration at tree and canopy scales, providing independent data for flux comparisons and model validation in ecological and hydrological research (Wilson *et al.* 2001; Köstner *et al.* 2017). When integrated with long-term micrometeorological data, which encompasses microclimatic variables such as air temperature and relative humidity recorded at the study site (Köstner *et al.* 2017; Delapierre *et al.* 2024), sap flow time series support cross-validation of water vapor and latent heat fluxes and

improve inference on plant water status and transport dynamics, including age-related patterns in managed forest stands (Köstner *et al.* 2017). Although sap flow responses can be dampened or time-lagged relative to atmospheric demand - as reflected by vapor pressure deficit (VPD), an environmental factor derived from air temperature and relative humidity that represents the evaporative driving force for water movement (Balducci *et al.* 2020) - and driven by the depletion and replenishment of internal water storage (Steppe *et al.* 2015a; Oogathoo *et al.* 2020), they remain informative indicators of whole-tree water use (Steppe *et al.* 2016; Köstner *et al.* 2017; Oogathoo *et al.* 2020). Furthermore, these high-resolution measurements can track longer-term physiological adjustments and potential recovery following forest disturbances (Granier 1985; Balducci *et al.* 2021a).

Under defoliation, Balducci *et al.* (2020) suggest that tree responses to long-term (>5 years) defoliation, particularly water uptake and the ability to regulate water status, are inadequately studied under field conditions in boreal forests. Defoliation severity and duration are critical factors for leaf gas exchange in conifers affected by prolonged defoliation (Salmon *et al.* 2015; Balducci *et al.* 2020). Research shows that active defoliation by larvae can negatively affect control of evaporative demand and reduce midday leaf water potential (Salmon *et al.* 2015; Bouzidi *et al.* 2019; Balducci *et al.* 2020). However, after defoliation (when larvae are not actively feeding), a positive effect on water balance was observed in the short term, increasing water potential (Balducci *et al.* 2020; Balducci *et al.* 2021a). In boreal conifers, defoliation over a two-year period can rapidly enhance tree water status and reduce growth loss (Bouzidi *et al.* 2019; Balducci *et al.* 2021a). These findings indicate that the impacts of defoliation are time-dependent, transitioning from beneficial in the short term to detrimental when the duration exceeds 5–10 years (Paixao *et al.* 2019; Balducci *et al.* 2020; Balducci *et al.* 2021a). Generally, defoliation negatively influences tree water status by reducing plant water potential (Salmon *et al.* 2015; Grüning *et al.* 2017; Balducci *et al.* 2020; Zhang *et al.* 2021). In black spruce, the reduction in leaf water potential is more influenced by defoliation than by vapor pressure deficit, whereas the reduction in tree water potential in balsam fir was explained by both biotic and abiotic factors (Balducci *et al.* 2020).

Defoliation triggers a spectrum of physiological adaptations, primarily through the preferential reallocation of carbon from secondary stem wood and root growth toward the restoration of foliage and photosynthetic capacity (MacLean 2016; MacLean *et al.* 2024). Growth-ring declines during insect outbreaks are well documented, with defoliation inducing immediate and significant suppressions in radial increment (Morin 1994; Axelson *et al.* 2014; Pandeya *et al.* 2026). Morin (1994) identified exceptionally narrow rings (or series of narrow rings), which represent pronounced periods of growth suppression (Axelson *et al.* 2014; Pandeya *et al.* 2026), followed by growth recovery following spruce budworm outbreaks. He also reported many missing or incomplete rings in trees affected by recurrent outbreaks (Blais 1958; Morin 1994; MacLean 2016). In spruce, severe defoliation occurs primarily during periods of high spruce budworm population density, where black spruce can experience a median growth shift of -64.38% in surviving trees and declines of approximately -90% in trees that die (Pandeya *et al.* 2026). In contrast, balsam fir exhibits more consistent and severe growth reductions, with declines typically ranging from 50% to 75% in radial and volume increments (Piene 1980; MacLean 2016; MacLean *et al.* 2024).

Growth reduction under defoliation can also be studied by continuously monitoring stem radius variation (SRV) using automatic point dendrometers. These instruments record reversible contractions and expansions of elastic stem tissues, primarily the sum of bark and xylem variation, driven by transpiration-induced water depletion and subsequent replenishment (De Swaef *et al.* 2015; Zweifel *et al.* 2021). These data are also useful for studying environmental controls on tree water status and growth dynamics (Oogathoo *et al.* 2023). By partitioning stem radius variation into growth and water-related components, dendrometers characterize summer radial expansion (Oogathoo *et al.* 2023) and tree water relations (De Swaef *et al.* 2015; Zweifel *et al.* 2021), as well as cold-season processes such as autumn dehydration, winter freezing, and spring rehydration (Turcotte *et al.* 2009; Delapierre *et al.* 2024). During summer, stem growth is commonly quantified using the zero-growth concept, which defines growth as an irreversible process occurring only when the measured stem radius exceeds the running maximum reached up to that time (Zweifel *et al.* 2016; Zweifel *et al.* 2021). By separating reversible fluctuations of the extensible tissues of the bark (comprising the phloem and cambium) driven by tree water status (Steppe *et al.* 2006; Zweifel *et al.* 2016), this approach allows

the identification of growth pulses at hourly resolution. These pulses occur predominantly when tissues are fully hydrated (maximum turgor) and under low atmospheric demand, typically during the night, a pattern consistently observed across a broad range of both coniferous and deciduous temperate tree species (Deslauriers *et al.* 2007; Zweifel *et al.* 2016; Zweifel *et al.* 2021). Dendrometers enable continuous, non-destructive monitoring at the same location on the trunk and provide uninterrupted high-resolution seasonal time series that serve as indirect proxies for the temporal dynamics of wood formation (Deslauriers *et al.* 2003; Steppe *et al.* 2016; Oogathoo *et al.* 2023). Under defoliation, a reduction in summer stem-radius increase is expected due to reduced tree-ring formation (Morin 1994). However, it remains unknown whether the decreasing growth and water status under defoliation can have an impact on the winter and spring process in impacted trees.

Winter stem contraction, or winter shrinkage, recorded by point dendrometers represents a thermal signal, as winter stem diameter variations integrate freeze–thaw processes - defined as the cyclic formation and melting of ice within the stem apoplast (Turcotte *et al.* 2009; Delapierre *et al.* 2024) - and changes in tree water status (De Swaef *et al.* 2015; Delapierre *et al.* 2024). While individual freeze–thaw events can produce reversible shrinkage via cellular water redistribution, as shown experimentally in walnut (Améglio *et al.* 2001), dendrometer series also serve as indicators of water status through the depletion of elastic water pools in the bark (De Swaef *et al.* 2015; Zweifel *et al.* 2016; Delapierre *et al.* 2024). Building on this, Delapierre *et al.* (2024) proposed that sustained winter shrinkage indicates “frost drought” driven by ice blockage due to frozen basal stem, while distal tissue lose some water during the day. Consequently, winter contraction may provide a practical proxy for winter desiccation which consists in chronic winter water stress in conifers (Delapierre *et al.* 2024).

Turcotte *et al.* (2009) emphasized defining key physiological periods based on tree physiological state, which can be achieved through analyses of stem and root radius variations. They identified three distinct periods based on these variations and their comparison with environmental variables (air temperature, soil temperature, snow depth, soil unfrozen water content): (1) winter shrinkage, (2) spring rehydration, and (3) summer transpiration. By graphically observing the stem radius variation data, it is possible to identify patterns suggesting a mathematical way to characterize these periods, following the approach of Tardif *et al.* (2001), who defined discrete seasonal phases

by graphically analyzing mean cumulative increments and first-difference indexed activity curves. This determination is important because defoliation may affect not only the amplitude of radial growth during summer, but also winter shrinkage and spring rehydration—potentially indicating reduced stem water recharge in spring that impacts tree water status, growth and thus tree vitality.

OBJECTIVES AND HYPOTHESES

In this study, we aimed to monitor sap flow and stem radius variation in two conifer species (black spruce and balsam fir) to improve our understanding of how a spruce budworm outbreak impacts their physiology across seasonal cycles (dehydration, freezing, rehydration and growth) over an eight-year period. We hypothesized (FIGURE 1) that (**i**) during years of active spruce budworm defoliation, the intensity of defoliation, occurring during the transpiration and growth period, is positively associated with the magnitude of reduction in sap flow (Qs) and stem radius variation in both species (balsam fir and black spruce), and that this effect extends across subsequent physiological periods; and (**ii**) climatic factors, represented by the vapor pressure deficit (VPD), modulate the relationship between tree transpiration and spruce budworm defoliation. Under conditions of high defoliation, elevated evaporative demand (high VPD) is expected to further reduce transpiration and consequently stem radius variation.

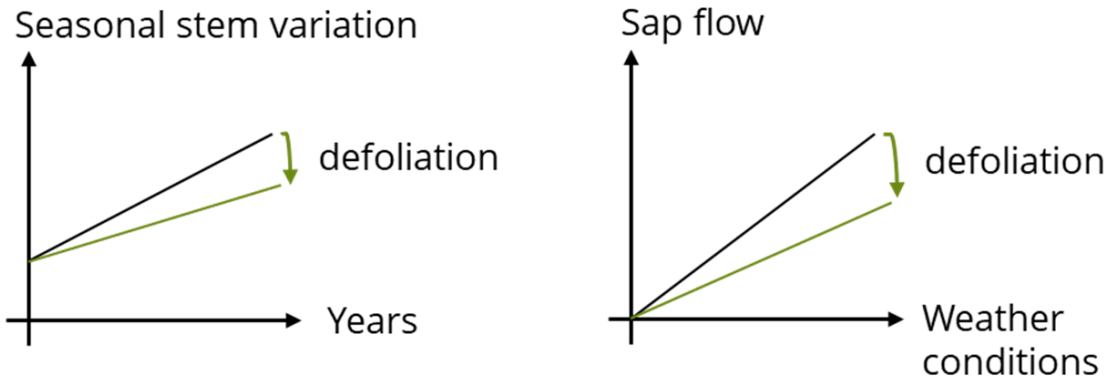

FIGURE 1 : Conceptual illustration of the hypothesized defoliation effect on stem dynamics and water use. Relative to non-defoliated years (black), active spruce budworm defoliation (green) is expected to reduce (left) seasonal stem radius variation, defined here as the amplitude of each phase, and (right) transpiration across comparable weather conditions, leading to lower values over the defoliation period.

CHAPITRE 1
MATERIALS AND METHODS

1.1 STUDY SITE

The data were collected in a permanent plot named Gaspard located at the Monts-Valin National Park (QC, Canada) (48° 34' N 70° 53' W), located at 227 m above sea level (a.s.l.) (FIGURE 2). Monts-Valin National Park is a protected area established to conserve and enhance representative natural ecosystems of Quebec (Sépaq 2024). This area is predominantly populated by balsam fir [*Abies balsamea* (L.) Miller] and black spruce [*Picea mariana* (Mill.) BSP], with additional tree species such as white spruce (*Picea glauca* Moench.), birch (*Betula papyrifera* Marshall.), and aspen (*Populus tremuloides* Michx.) but of lower abundance as elevation increases (Huang et al. 2014). Stand and tree characteristics of the two main conifer species at Gaspard are presented in TABLE 1. Gaspard is situated within the balsam fir-yellow birch forest bioclimatic domain, which spans a region of approximately 98,600 km² across Quebec (Saucier et al. 2009). Between 1991 and 2020, the region experienced average daily temperatures ranging from -15.1°C in January to 18.7°C in July, with extremes recorded at -40.6°C (January 2014) and 38.4°C (July 2002) (ENR 2024). The annual precipitation average is 927.7 mm, and the frost-free period lasts approximately 128 days, supporting a short growing season (ENR 2024). Natural disturbances, including spruce budworm (*Choristoneura fumiferana*) outbreaks and occasional low-intensity fires, significantly influence forest structure and regeneration, fostering a diverse mix of species adapted to both shade and disturbance dynamics (Saucier et al. 2009).

TABLE 1 : Stand and tree characteristics of black spruce and balsam fir at the Gaspard site. Mean tree height was obtained from Huang *et al.* (2014), mean stand age was updated to 2024 from the values reported by Huang *et al.* (2014), and DBH was calculated from measurements collected in 2024 in the present study.

Species	**Mean stand age (years ± SD)**	**Mean tree height (m ± SD)**	**Mean DBH (cm ± SD)**
Black spruce	51 ± 3.7	14.2 ± 1.6	25.66 ± 4.46
Balsam fir	61 ± 3.7	17.6 ± 2.6	27.36 ± 4.06

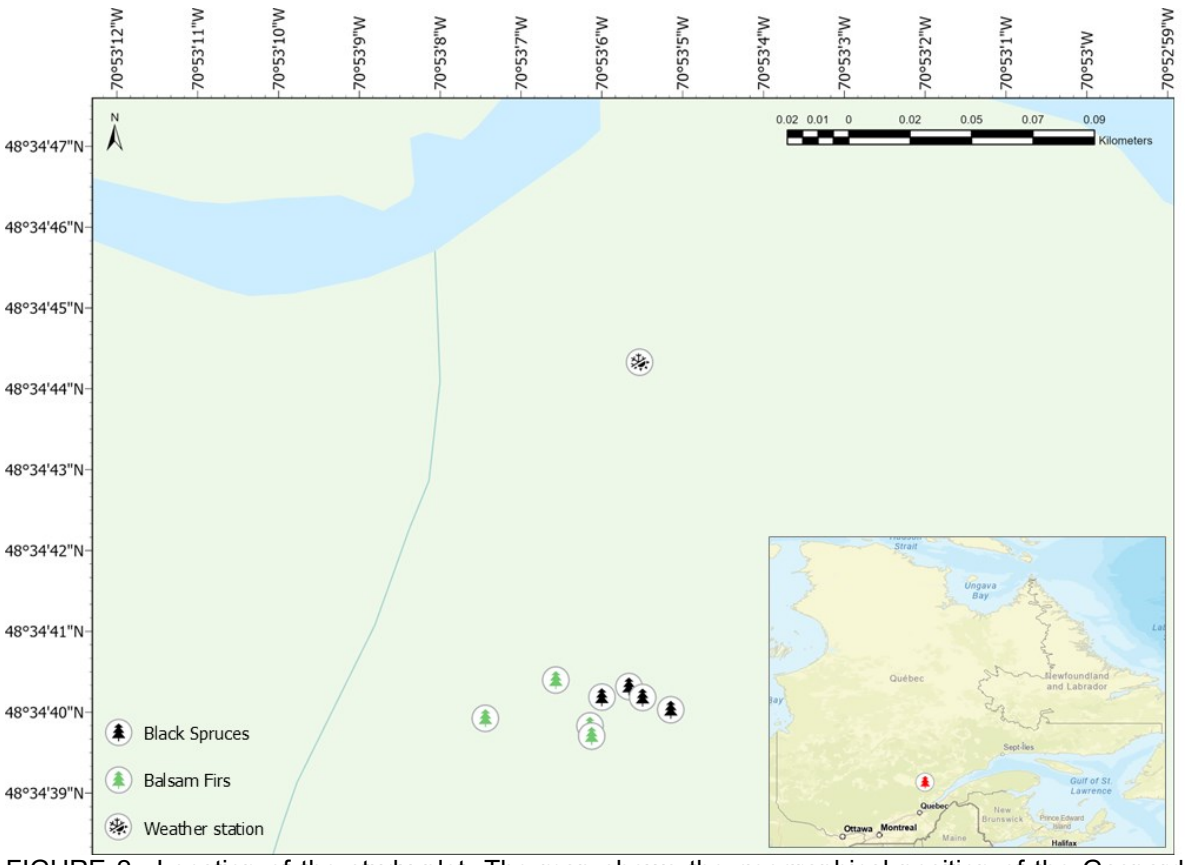

FIGURE 2 : Location of the study plot. The map shows the geographical position of the Gaspard study site (48°34′N, 70°53′W) within the Monts-Valin National Park, Québec, Canada. The inset map indicates the location of the study area in the province of Québec (red tree symbol). Individual monitored trees are represented by icons: black spruces (black trees), balsam firs (green trees), and the weather station (snowflake symbol).

1.2 DATA COLLECTION

1.2.1 DENDROMETERS DATA

The stem radius variation of eight trees – four balsam firs (BF) and four black spruces (BS) – was monitored using point dendrometers (Ecomatik, Munich, Germany), forming a continuous time series from May 2017 to October 2024. These sensors were installed at approximately 1.3 meters above ground level on the north side of the trunks, which remained above the seasonal snow cover, as snow depth at the site does not exceed 1.3 m. Measurements were recorded every 15 minutes and logged using CR1000 data loggers (Campbell Scientific Corporation, Logan, UT, USA). The

dendrometer equipment, connected to the data logger, provided a resolution of 0.2 µm and an accuracy of 1.5 µm.

1.2.2 FLUXMETERS DATA

The sap flow sensors used in our research were custom-built at the university (Balducci *et al.* 2021a). These sensors were developed following the design proposed by Granier (1985), based on the heat dissipation method. This method measured the temperature difference (ΔT) between two probes, using a thermocouple (Nordic Sensors Industrial Inc., CA) composed of two dissimilar conductors forming electrical junctions at different temperatures: one with a constant heating, and other serving as a temperature reference. They were installed annually on the same trees from approximately May to October (2018 to 2024). Data were recorded at 15-minute intervals and stored using CR1000 data loggers (Campbell Scientific Corporation, Logan, UT, USA).

The heat dissipation method to measure sap flow (Granier 1985) consists in two cylindrical probes, each 2 mm in diameter, inserted 2 cm into the sapwood on the north side of the tree trunk. These probes were insulated with thermal material to shield them from direct sunlight and external temperature fluctuations. One probe was positioned 10 cm above the other, with each probe equipped with a T-type thermocouple for temperature measurement, connected in opposite directions. The probe pairs were installed at a height of approximately 1.8 meters to minimize potential interference from variations in stem radius measured with the dendrometer. The upper probe was consistently heated at a constant power of 0.2 W, while the lower probe remained unheated to serve as a reference for the wood tissue temperature (Balducci *et al.* 2021b).

1.2.3 METEOROLOGICAL DATA

The meteorological data were collected from a standard weather station located near the experimental plot. The station consists of a 10 m tower equipped with a CR1000 datalogger

(Campbell Scientific Corporation, Logan, UT, USA), which records 5-minute measurements and stores them as hourly averages for the following variables: maximum and minimum air temperature (°C) and relative humidity (%) measured with a HygroVue™10 sensor, and precipitation (mm) measured with a CS700 sensor.

1.2.4 DEFOLIATION DATA

We obtain spruce budworm defoliation data in Québec through annual aerial surveys conducted by the *Ministère des Forêts, de la Faune et des Parcs* (MFFP) (DPF 2025). The affected areas are delimited in flight on a 1:50 000 topographic map that follows the aircraft's route. Defoliation was classified according to the yearly foliage loss of the canopy of the main host species (balsam fir, white spruce, and black spruce). So, no distinction was made between the species. Four defoliation classes were recorded as a defoliation index measured for the given year named DI (defoliation index) field (MRNF 2023): 0-Absence of defoliation (detection by Sentinel images), 1-Light (loss of foliage in the upper third of the crown of a few trees; 1-34%), 2-Moderate (loss of foliage in the upper half of the crown of the majority of trees; 35-69%), and 3-Severe (loss of foliage along the entire length of the crown of the majority of trees; 70-100%). Data were available in FGDB format, with global and regional annual summaries (DPF 2025).

Using the annual defoliation index (DI) values, we calculated the cumulative defoliation index ($DI_{cumulative}$) (MRNF 2023) for our region, as the sum of the annual DI values from 2016 to 2024:

$$DI_{cumulative} = \sum_{t=2016}^{2024} DI_t. \quad \text{Eq 1}$$

Thus, $DI_{cumulative}$ represents the accumulated defoliation severity over the study period rather than that of a single year. Accordingly, values can exceed 3 because the index is the sum of annual DI values across years. In this study, $DI_{cumulative}$ therefore provides an integrated measure of the recurrence and intensity of defoliation from 2016 to 2024.

1.3 MATHEMATICAL ANALYSES

1.3.1 DENDROMETER DATA ANALYSES

Because of the variation in the climate and extreme weather data between the summer and the winter, the dendrometer series were first separated into distinct periods following the phenological cycles through the year (Turcotte *et al.* 2009) representing a seasonal macro analysis. All data processing and analyses were performed using the Python programming language version 3 (Van Rossum et Drake 2009).

We applied cubic spline interpolation using the *CubicSpline* function from the SciPy library in Python (Virtanen et al. 2020) to address the missing values in the dendrometer time series, which did not exceed one day. This method reconstructed gaps based on the surrounding observations, ensuring continuity in the dataset. Additionally, the interpolation process was restricted to avoid extrapolation beyond the observed data range.

After addressing the missing values, we smoothed the time series using a non-parametric model: the cubic smoothing spline (Spline Model), adopting the *UnivariateSpline* function from the SciPy library (Virtanen et al. 2020). This approach fits piecewise cubic polynomials to the data points through an optimization process that balances the proximity of the curve to the data points, measured by the root mean square (RMS) distance, with a penalty for excessive curvature to prevent overfitting (Dusart et al. 2024). The smoothing parameter (*s*) was optimized according to the tree species, with values set to 370 for Spruce and 95 for Fir. These values were chosen empirically, considering both root mean square (RMS) and curve shape, to balance flexibility with preservation of growth trends; specifically, they are the smallest *s* values that still allow reliable identification and classification of inflection points marking the onset of seasonal phases, without over smoothing the biological changes over the season.

Using the smoothing function, we identified inflection points by calculating the second derivative of the smoothed curves (*see the next paragraphs for the mathematical definition of the phases*). We observed that some of these inflection points, as determined through visual graphical

analysis and supported by previous studies (Tardif et al. 2001; Turcotte et al. 2009), coincided with significant changes in the behavior of the stem radius variation along the year. In other words, it was possible to identify the beginning of each period with an inflection point. These points were then used to define the starting points of five annual periods: (1) winter dehydration, (2) freezing state, (3) spring rehydration, (4) transpiration and growth, and (5) end of transpiration and growth (FIGURE 3).

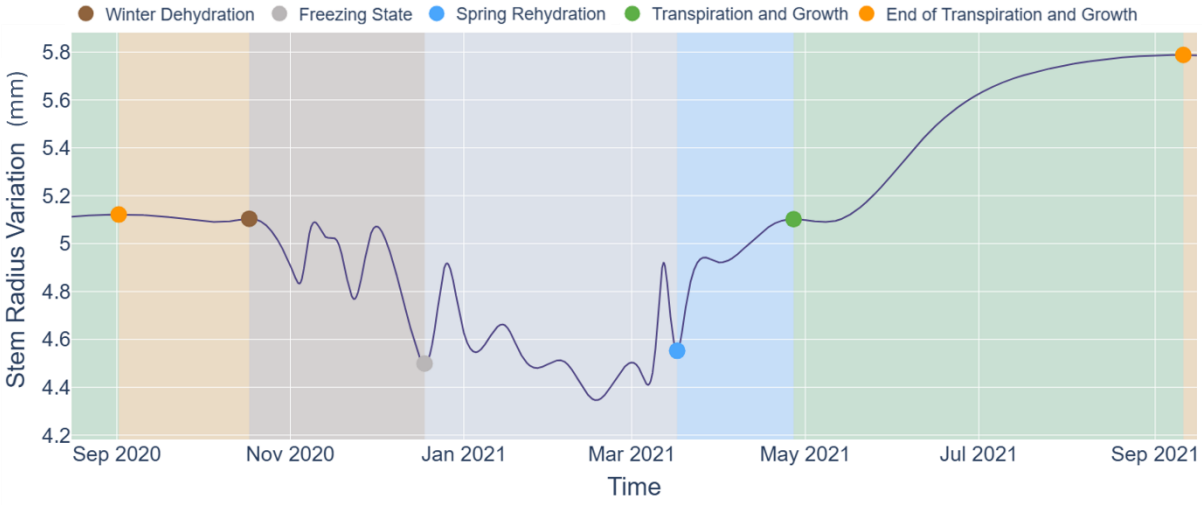

FIGURE 3 : Sketch of a time series of the smoothed stem radius variation of a balsam fir between September 2020 and September 2021. The seasonal trends in stem radius variation are divided into five distinct periods: (1) winter dehydration (brown), (2) freezing state (gray), (3) spring rehydration (blue), (4) transpiration and growth (green) and (5) end of transpiration and growth (orange). The transition between periods is represented by a colored dot, and the rectangle of the same color in the sequence indicates the duration of that period.

To filter and select the inflection points that mark the beginning of each phenological period in the seasonal variation of the stem radius, were defined five functions $\left(t_{q,a}^{SR}, t_{q,a}^{TG}, t_{q,a}^{ETG}, t_{q,a}^{WD}, t_{q,a}^{FS}\right)$, where *t* denotes the event time (*timestamp*) returned by the selection procedure. Each function takes as input the processed dendrometer time series $x_q(t)$ and a dictionary of candidate inflection points previously classified as local maxima, local minima, or intermediate inflections. For each tree *q* and year *a*, the function returns the timestamp (YYYY–MM–DD hh:mm:ss) of the event selected for the corresponding period, and its associated amplitude when applicable; outputs are stored in a dictionary indexed by tree. In addition, for each period we imposed a search window $I_{q,a}$ (TABLE 2) adapted from Turcotte *et al.* (2009), to ensure that the selected onset time falls within the expected seasonal interval for each year.

TABLE 2 : Stem phenological intervals (start date - end date) used as calendar windows for each function to identify the starting point of the physiological periods in stem radius variation measured with point dendrometers. In some cases, it was necessary to differentiate the dates between species to respect their physiological and phenological responses.

Periods	Species	Start Date	End Date
Spring rehydration	Spruce	10th March	20th April
	Fir		15th April
Transpiration and growth	Spruce	26th April	7th June
	Fir	20th April	31st May
End of transpiration and growth	Spruce	1st July	15th September
	Fir		
Winter dehydration	Spruce	20th October	25th November
	Fir	15th October	30th November
Freezing state	Spruce	20th November	31st December
	Fir	10th November	

For the Spring Rehydration period, we first defined the set of candidate minima $M_{q,a}^{min}$ occurring within the spring rehydration window $I_{q,a}$ (TABLE 2) for each tree *q* and year *a*. For any candidate minimum at time $t \in M_{q,a}^{min}$, we identified the first subsequent maximum $t_{max,q}^{+}(t) = \min\{s \in M_{q,a}^{max} : s > t\}$, where *s* denotes a generic candidate timestamp among the local maxima of series *q*. We then computed the associated amplitude as $A_q(t) = x_q\left(t_{max,q}^{+}(t)\right) - x_q(t)$. The start of spring rehydration was then defined as $t_{q,a}^{SR} = \arg\max_{t \in M_{q,a}^{min}} |A_q(t)|$, with the reported amplitude $A_{q,a}^{SR} = A_q\left(t_{q,a}^{SR}\right)$. This choice corresponds to the moment when stem radius reaches its lowest value prior to the subsequent expansion phase.

For the Transpiration and Growth period, we first restricted the analysis to its respective window $I_{q,a}$ for each tree *q* and year *a*. Within $I_{q,a}$, (TABLE 2) we defined the set of candidate onset points $C_{q,a} = M_{q,a}^{max} \cup M_{q,a}^{inf}$, where $M_{q,a}^{max}$ denotes local maxima and $M_{q,a}^{inf}$ denotes intermediate inflection points (excluding minima). For any candidate point at time $t \in C_{q,a}$, we identified the closest minimum immediately to the left, $t_{min,q}^{-}(t) = \max\{u \in M_{q,a}^{min} : u < t\}$, and computed the associated amplitude as $A_q(t) = x_q(t) - x_q\left(t_{min,q}^{-}(t)\right)$. The start of the Transpiration and Growth period was then defined as $t_{q,a}^{TG} = \arg\max_{t \in C_{q,a}} A_q(t)$, with the reported amplitude $A_{q,a}^{TG} = A_q\left(t_{q,a}^{TG}\right)$. This criterion

selects, within each year, the maximum (or intermediate inflection) associated with the largest increase in stem radius relative to the preceding minimum.

For the End of Transpiration and Growth period, we first restricted the analysis to its respective window $I_{q,a}$ (TABLE 2) for each tree *q* and year *a*. Within $I_{q,a}$, we considered the full set of classified inflection points $K_{q,a} = M_{q,a}^{min} \cup M_{q,a}^{max} \cup M_{q,a}^{inf}$ and selected the point with the highest stem radius value, $t_{q,a}^{ETG} = \arg\max_{t \in K_{q,a}} x_q(t)$, reporting the corresponding value $x_q\left(t_{q,a}^{ETG}\right)$. This point represents the last major stem expansion peak before the onset of winter dehydration.

For the Winter Dehydration period, we first restricted the analysis to the winter dehydration window $I_{q,a}$ (TABLE 2) for each tree *q* and year *a*. Within $I_{q,a}$, we identified all candidate maxima $t \in M_{q,a}^{max}$ and, for each maximum, we searched for the first subsequent minimum $t_{min,q}^{+}(t) = \min\{u \in M_{q,a}^{min} : u > t\}$. We then computed the associated contraction amplitude as $A_q(t) = \left| x_q\left(t_{min,q}^{+}(t)\right) - x_q(t) \right|$. Among all maximum-minimum pairs, we retained the two largest amplitudes and defined the start of Winter Dehydration as the earliest maximum time among these two events, $t_{q,a}^{WD} = min\{t \in M_{q,a}^{max} : A_q(t)\ is\ among\ the\ two\ largest\ values\}$, with the reported amplitude $A_{q,a}^{WD} = A_q\left(t_{q,a}^{WD}\right)$. This criterion selects the earliest major stem contraction within the dehydration window.

Finally, for the Freezing State period, we first restricted the analysis to the freezing-state window $I_{q,a}$ for each tree *q* and year *a*. Within $I_{q,a}$, (TABLE 2) we defined the set of candidate minima $M_{q,a}^{min}$ and, for each minimum at time $t \in M_{q,a}^{min}$, we identified the closest maximum immediately to the left, $t_{max,q}^{-}(t) = \max\{s \in M_{q,a}^{max} : s < t\}$. We then computed the associated amplitude as $A_q(t) = x_q(t) - x_q\left(t_{max,q}^{-}(t)\right)$. The start of freezing state was defined as the minimum time $t_{q,a}^{FS} = \arg\max_{t \in M_{q,a}^{min}} \left| A_q(t) \right|$, with the reported amplitude $A_{q,a}^{FS} = A_q\left(t_{q,a}^{FS}\right)$. This criterion selects the minimum associated with the largest contraction relative to the preceding maximum within the freezing-state window.

Maintaining a seasonal perspective, it was assumed that each period ends at the exact moment the next begins. With this in mind, we derived several key metrics for each period: (1) the Start and End dates of each period, along with their respective values, which were derived directly

from the inflection points; (2) the Seasonal Delta (named *Δseasonal*, mm), calculated as the difference between the values on the End Date and Start Date for each period; (3) the Duration in days (d), determined as the difference between the End and Start Dates; (4) the Maximum and Minimum values within each period, along with their respective dates; and (5) the Intra-seasonal Delta, calculated as the difference between the Maximum and Minimum values for each period (mm).

An ANOVA was used to test for differences in mean Δ*seasonal* between species (black spruce vs. balsam fir) and among years using the model:

$$\Delta seasonal = \mu + Species + Year + \varepsilon, \quad \text{Eq 2}$$

where μ is the overall mean, Species and Year are the categorical fixed effects, and ε is the residual error term. This analysis was followed by two contrast tests.

In both contrasts, the levels (x_i) were defined based on the cumulative defoliation index (DI) for each year (i), separately for each period analyzed. The linear contrast coefficients (c_i) were obtained by centering (x_i) relative to the mean of the years available within each period, i.e., $c_i \propto x_i - \bar{x}$. To avoid fractional coefficients, the equivalent integer form $c_i = nx_i - \sum x$ was used (where *n* is the number of years present in that period), ensuring $\sum c_i = 0$; the coefficients were then simplified by dividing all values by the greatest common divisor of the non-zero coefficients. The first contrast included all years and aimed to assess the temporal trend. Because 2020 was the only year with DI=3, it was treated as a turning point. Accordingly, the second contrast tested the difference between the pre-2020 mean (2017-2019) and the post-2020 mean (2021-2024).

To determine whether stem radius variation during one phenological phase could statistically anticipate and influence the subsequent phase, we applied the Granger causality test (Granger 1969) to the Seasonal Delta values of each species. This test evaluates whether past information from one time series improves the prediction of another, identifying potential cause–effect relationships over time. Pairwise Granger tests were performed among all periods combinations to detect directional dependencies, using the *grangercausalitytests()* function from the *statsmodels* library (Seabold et Perktold 2010). A maximum lag of one year (max_{lag} = 1) was adopted to test short-term interannual dependencies while maintaining sufficient degrees of freedom given the available years (n = 7).

Statistical significance was assessed at $p < 0.05$ based on the chi-squared statistic [Sum of Squared Residuals (SSR) test)].

To evaluate temporal consistency between phenological periods identified from seasonal variations in stem radius, we calculated pairwise correlations between periods for each species. Since extreme values can distort correlations estimates, we conducted an influence analysis for each pair of periods and species. This step allowed us to identify potentially influential years based on three criteria: (1) z-score values ≥ 3 in any of the variables; (2) Cook's distance ($D > 4/n$); and (3) leverage ($h_{ii} > 2p/n$) combined with studentized residuals ($|r| > 3$). After excluding the influential years, we recalculated the correlations to compare the coefficients obtained with and without the influential points. The analyses included parametric (Pearson), nonparametric (Spearman), and robust (Theil–Sen) approaches, ensuring a comprehensive assessment of the relationships between phenological periods.

1.3.2 FLUXMETER DATA ANALYSES

The recorded temperature differences (ΔT, ℃) from the sensors were converted into sap flow density (F_D, g/(cm²·h)) using the original calibration equation by Granier (1985); (1987):

$$F_D = \alpha \cdot K^{\beta}, \quad \text{Eq 3}$$

where α = 42.84 and β = 1.231 are equation parameters (Niu et al. 2015), and K is defined as:

$$K = \frac{\Delta T_{max} - \Delta T}{\Delta T}, \quad \text{Eq 4}$$

where ΔTmax (℃) is the maximum daily value between 0h and 6h.

Subsequently, we computed the hourly average of sap flow density (F_D, g·cm^{-2}·h^{-1}), for each tree and integrated the hourly series using the trapezoidal rule to obtain daily sap-flow density (g·cm^{-2}·d^{-1}). We then converted daily F_D to volumetric sap flow (Q_S, L·day^{-1}) by scaling with active sapwood area (Eq 6):

$$Qs = \frac{F_D \cdot Sapwood\ Area}{1000}, \quad \text{Eq 5}$$

assuming a water density of 1000 g·L^{-1}.

Where sapwood area was estimated using the allometric equation of Bond-Lamberty et al. (2002):

$$\log_{10}(Y) = a + b(\log_{10}(D) + c(AGE) + d(\log_{10}(D) \cdot AGE), \quad \text{Eq 6}$$

where Y is sapwood area (cm^2), D is stem diameter (cm), AGE is stand age (years); the cross product represents the interaction between diameter and age. We assumed the same coefficients (Bond-Lamberty et al. 2002) for both species: a = -0.451, b = 2.442, c = 0.002 and d = -0.007. Based on Huang et al. (2014), stand age (mean, SD) in our region is 40 ± 3.7 years for spruce and 50 ± 3.7 for fir.

1.3.3 MIXED EFFECTS MODEL FOR Q_S (L/day)

To evaluate how the mean seasonal stem diameter increment (Δseasonal) influenced the mean water use (Qs), we performed a linear regression of the form Qs∼Δseasonal. Because water use depends on atmospheric demand (VPD), it was necessary to remove the influence of VPD to test how spruce budworm could alter both the slope and the intercept of these relationships across years. To improve the distribution and residuals, we applied a Box-Cox transformation to the Qs values. Since this transformation does not allow zeros, we added a shift of 10^{-6} to enable the transformation. The Box-Cox λ parameter was estimated empirically from the data. Observations with missing values in Qs, VPD, Year, Species, or Tree were excluded. We then modeled volumetric sap flow (Qs, L/day) at the tree level using a linear mixed-effects model [MixedLM; statsmodels (Seabold et Perktold 2010)]. Year and Species were treated as categorical variables, and a random intercept was specified for each tree (group = Tree) to capture individual heterogeneity (structural and instrumentation differences). Fixed effects for Year, VPD, Species, and their interactions of VPD with Species and Year were tested, according to:

$$Q_s \sim Year + VPD * Species + VPD{:}Year \quad \text{Eq 7}$$

In this model specification, 2018 is the reference year and spruce the reference species (with fir coded by contrast). The VPD*Species term includes the main effects of VPD and Species as well as their interaction, allowing species-specific VPD slopes (climate sensitivity), while VPD:Year allows

year-specific slopes (interannual modulation of the VPD response). The model was adjusted by maximum likelihood (ML; reml=False), with fallback to the L-BFGS optimizer if convergence issues occurred, to facilitate inference and pairwise contrasts on the fixed effects.

CHAPITRE 2
RESULTS

2.1 ACCUMULATED DEFOLIATION

The cumulative defoliation increased almost continuously from 2016 to 2024 in the study region (FIGURE 4). A severe defoliation index (DI = 3) was recorded in 2020, according to the aerial survey of damage caused by the main insects and diseases that attack trees (DPF 2025). In all other years within our study region, defoliation caused by spruce budworm was categorized as light (DI=1). In 2015 no defoliation was identified (DI = 0). The cumulative defoliation from 2016 to 2024 shown a progressive increase of leaf loss, but this accumulated defoliation presents a greater increase from 4 in 2019 to 7 in 2020.

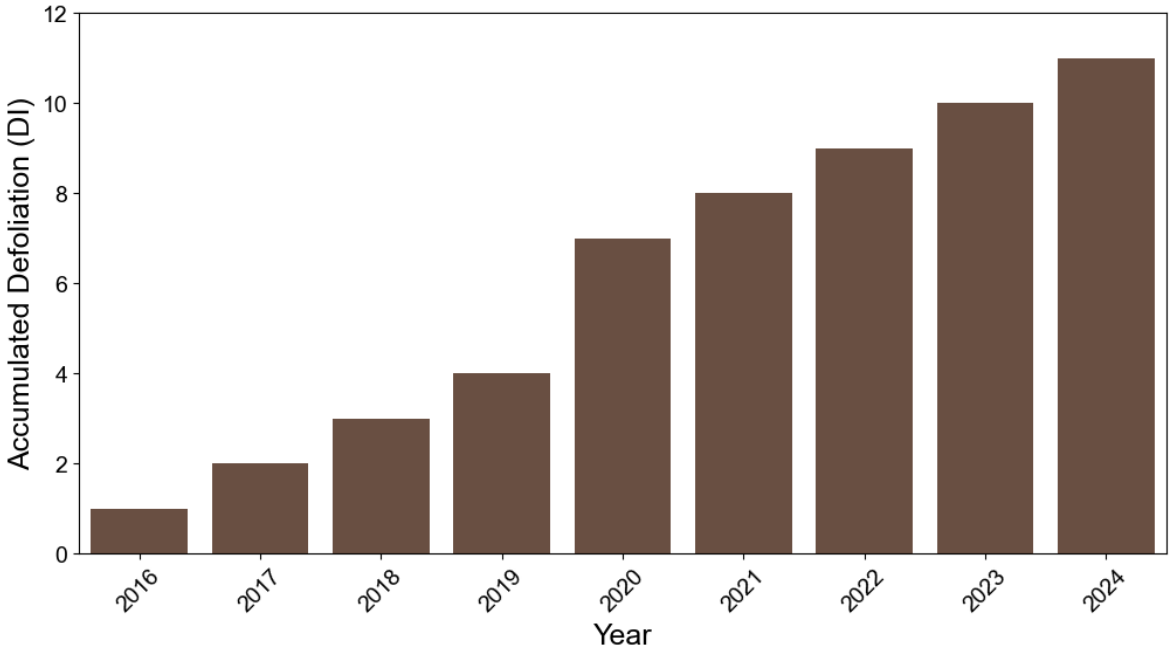

FIGURE 4 : Cumulative spruce budworm defoliation index ($DI_{cumulative}$) in the study plot from 2016 to 2024. Values represent the sum of annual defoliation index (DI) scores derived from aerial surveys; therefore, the cumulative index increases over time and may exceed the annual DI scale (0–3). The strongest increase occurred in 2020, corresponding to the only year with severe defoliation (DI = 3).

2.2 INTERANNUAL AND INTER-SPECIES DIFFERENCES

Stem radius variation exhibited consistent seasonal patterns across years (FIGURE 5; TABLE 3), with the studied species showing similar behavior and a degree of synchrony in the onset of the defined periods. These time series also display both interannual and within-season dynamics, including the mean duration of each period for each species, and the correspondent day of year (DOY) marking the onset of each period. Based on the fitted five distinct phenological phases shared by both species, the Winter dehydration (WD) phase lasted approximately 35 days for both species, beginning around day 310 and ending near day 345. This period was followed by Freezing state (FS) which extend for 112 days in black spruce, but about two weeks shorter in balsam fir, occurring from day 345 to day 92 of the following year. The Spring Rehydration phase (SR) began as temperature increased, lasting 35 and 43 days in balsam fir and black spruce, respectively. However, balsam fir tended to initiate spring rehydration earlier. The Transpiration and Growth (TG) phase persisted for about 110-112 days in both species, starting between day 126 and 132 and ending 237 and 244. Overall, balsam fir tended to initiate spring rehydration earlier and maintain growth activity slightly longer into autumn compared to black spruce (TABLE 3).

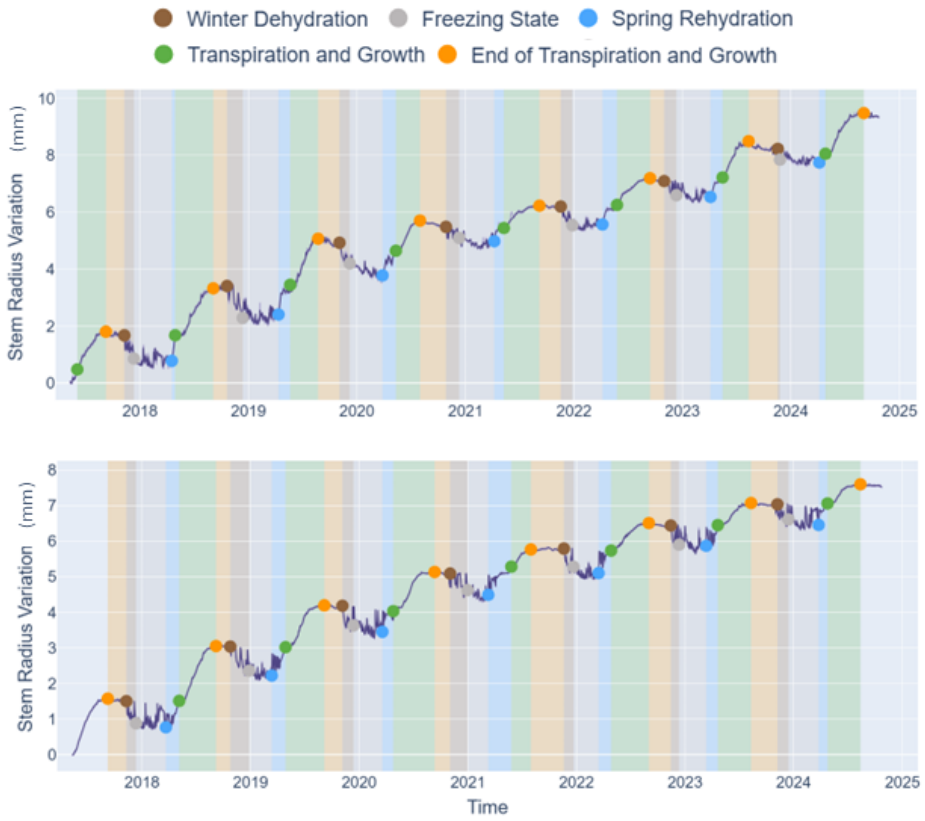

FIGURE 5 : Stem radius variations across five annual periods. The upper panel corresponds to Black Spruce, showing the temporal dynamics over all analyzed years, whereas the lower panel presents the same analysis for balsam Fir.

TABLE 3 : Mean stem phenological duration (days) and estimated start and end dates (DOY ± SD) for each period and species, based on the five defined phenological phases identified from stem radius variation time series.

Period	Species	Duration (days)	Start DOY ± SD	End DOY ± SD
Winter Dehydration (WD)	Spruce	34.6	310 ± 8.9	345 ± 8.6
	Fir	34.9	312 ± 8.0	347 ± 9.9
Freezing State (FS)	Spruce	111.8	345 ± 8.8	92 ± 11.4
	Fir	97.6	347 ± 9.9	80 ± 8.3
Spring Rehydration (SR)	Spruce	35.4	92 ± 11.4	128 ± 12.0
	Fir	43.0	80 ± 8.3	123 ± 13.7
Transpiration and Growth (TG)	Spruce	111.7	132 ± 14.4	244 ± 12.8
	Fir	110.3	126 ± 14.2	237 ± 19.6
End of Transpiration and Growth (ETG)	Spruce	64.4	244 ± 12.6	308 ± 9.3
	Fir	71.7	238 ± 19.4	310 ± 9

In both species, most of the defined seasonal phases showed a significant reduction in their amplitudes as cumulative defoliation increased, except for the Freezing State (FIGURE 6). This

decreasing pattern was further supported by contrast tests assessing whether seasonal stem radius variation phases tracked the cumulative defoliation trajectory across all years, and whether 2020 (DI = 3) represented a turning point (TABLE 5). Significant interspecific variability was detected during the periods of winter dehydration ($F = 16.28$, $p = 0.0003$, TABLE 4), transpiration and growth ($F = 6.70$, $p = 0.0141$), and end of transpiration and growth ($F = 5.98$, $p = 0.0191$), showing decreasing amplitudes in fir. In addition, interannual variability was significant during three periods (TABLE 4), stem dehydration ($p = 0.005$), transpiration and growth ($p = 0.012$) and spring rehydration ($p < 0.0001$) indicating a shift in the amplitude of seasonal stem variation, mostly indicating a reduction most likely due to spruce budworm defoliation.

Indeed, as cumulative defoliation increased, stem dehydration tended to decrease (TABLE 5). This pattern was evident both in the linear trend across all observed years (linear estimate = 17.1479, $t = 4.6197$, $p < 0.001$) and in the comparison between the period before severe defoliation (2020, DI = 3) and the period after this defoliation level (linear estimate = 0.2375, $t = 4.2085$, $p < 0.001$). For fir, a steady decrease in Winter dehydration was observed, with a difference of 0.2 mm. For spruce, the decreasing trend was observed only in 2020, when the phase exhibited the highest value of delta, indicating less stem contraction during that winter (FIGURE 6c). The Freezing state then oscillated around zero throughout the analyzed years without any increasing or decreasing pattern. The following phase, spring rehydration, also decreases in amplitude: the contrast test supported a significant negative trend across years (linear estimate = −13.2461, $t = -2.3777$, $p = 0.0238$) and a significant shift between pre and post 2020 (pre-post estimate = −0.2249, $t = -2.4411$, $p = 0.0205$), but showed different patterns between species. While fir showed a steady decrease, from 0.936 in 2018 to 0.528 in 2023, spruce exhibited a slightly increase between 2018 and 2020, before starting to decrease. Similarly, the amplitude of transpiration and growth phase increased a little, before sharply declining, especially in the most defoliated year (2020), and the contrasts indicated an overall decrease across years (linear estimate = −17.7895, $t = -2.2131$, $p = 0.0337$) as well as a significant pre–post reduction (pre-post estimate = −0.5020, $t = -2.8346$, $p = 0.0041$). A recovery in growth amplitude was also observed during the last two years. Finally, a small decrease in the end of growth phase was observed (linear estimate = −2.6865, $t = -2.2682$, $p = 0.0289$), but

with more variation in spruce compared to fir (FIGURE 6). The variation in Seasonal Delta values (FIGURE 6) across these periods indicates a marked change in 2020 and 2021, coinciding with the period of highest defoliation and the subsequent year during the spruce budworm outbreak (FIGURE 4).

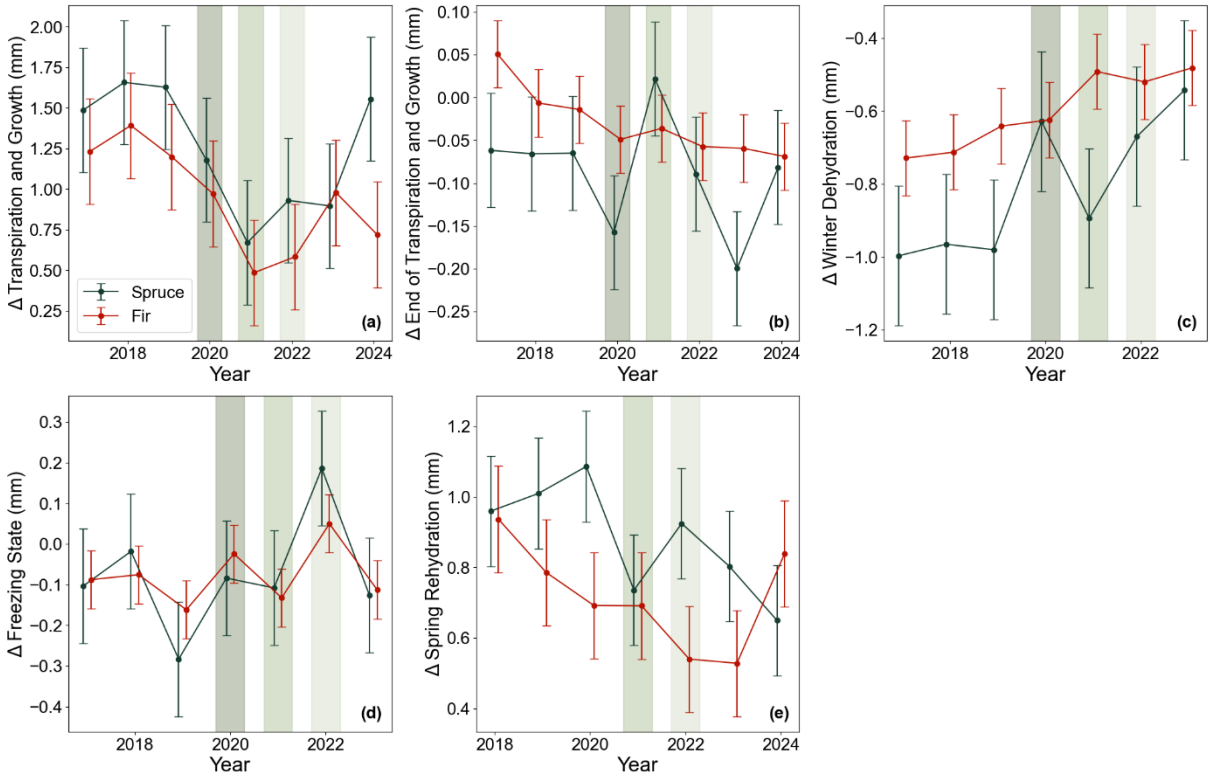

FIGURE 6 : Seasonal delta across the years. Each subplot represents one phenological phase, with a line for each species (red for balsam fir and dark green for black spruce). Vertical bars highlight the year of most severe defoliation (2020, in dark green) and the two subsequent years (2021 and 2022, in lighter green tones). The 2020 bar was not applied to spring rehydration because this phase occurred before the onset of the outbreak in that year, which began during the transpiration and growth period.

TABLE 4 : Effect of species and year on the variation of stem radius variation for the defined phenological period: Winter dehydration, Freezing state, Spring rehydration, Transpiration and growth and End of transpiration and growth.

Period	**Species**		**Years**	
	F (df)	P	F (df)	P
Winter dehydration	16.28 (1)	**0.0003**	3.83 (7)	**0.0051**
Freezing state	<0.01 (1)	0.9845	2.03 (7)	0.0883
Spring rehydration	3.13 (1)	0.0868	25.87 (7)	**<0.0001**
Transpiration and growth	6.70 (1)	**0.0141**	3.09 (7)	**0.0124**
End of transpiration and growth	5.98 (1)	**0.0191**	1.80 (7)	0.1156

TABLE 5 : Contrast results by period. Linear trend tests a gradual change over time (slope). Pre–post comparison tests a step change between two time blocks defined using 2020 as the turning point (DI = 3), comparing the mean difference post − pre. Estimate indicates effect magnitude and direction, SE the standard error, *t* the test statistic, *p* the significance value, and post-hoc power the a posteriori power (α = 0.05).

Period	Contrast type	Estimate	SE	t	p	Post-hoc power (α=0.05)
Winter Dehydration	Linear trend	**17.1479**	3.7119	**4.6197**	**< 0.001**	0.996
	Pre–post comparison	**0.2375**	0.0564	**4.2085**	**<0.001**	0.988
Freezing State	Linear trend	4.3822	3.9062	1.1219	0.2698	0.202
	Pre–post comparison	0.0810	0.0594	1.3637	0.1816	0.276
Spring Rehydration	Linear trend	**-13.2461**	5.5710	**-2.3777**	**0.0238**	0.662
	Pre–post comparison	**-0.2249**	0.0921	**-2.4411**	**0.0205**	0.684
Transpiration and Growth	Linear trend	**-17.7895**	8.0384	**-2.2131**	**0.0337**	0.600
	Pre–post comparison	**-0.5020**	0.1630	**-2.8346**	**0.0041**	0.868
End of Transpiration and Growth	Linear trend	**-2.6865**	1.1844	**-2.2682**	**0.0289**	0.621
	Pre–post comparison	-0.0444	0.0254	-1.0789	0.0880	0.417

2.3 TEMPORAL EFFECT

To better understand whether stem radius variation in one period anticipates and statistically influences the following phase in the annual cycle of each species, the Granger causality test applied once again revealed interannual dependencies (FIGURE 7). For Spruce, most relationships were not significant ($p>0.05$), indicating that few transitions between phases statistically explain the subsequent phase amplitude. However, two relationships showed significant causality, suggesting a coherent seasonal sequence: Spring Rehydration ($\chi^2=115.91$, $p<0.001$) and Transpiration and Growth ($\chi^2=7.24$, $p=0.0071$) influence the magnitude of the subsequent Winter Dehydration. These results indicate that, for Spruce, spring recovery and summer growth modulate the degree of stem shrinkage during the following winter.

In the case of Fir, the tests indicate a stronger temporal interdependence and carry-over effects across seasons. End of Transpiration and Growth influences the subsequent Spring Rehydration ($\chi^2=42.009$, $p<0.001$) and the degree of winter dehydration ($\chi^2=10.18$, $p=0.0014$), while Spring Rehydration affects Transpiration and Growth ($\chi^2=22.13$, $p<0.001$) and Winter Dehydration

(χ^2=66.20, p<0.001). In addition, Winter Dehydration modulates the following End of Transpiration and Growth (χ^2=22.959, p<0.001) and Spring Rehydration (χ^2=5.92, p=0.0149). Therefore, for Fir, the seasonal cycle is more interconnected and cyclical, reflecting a higher carry-over effect in both water dynamics and growth across the seasonal phases, including links between non-consecutive phases from one cycle to the next.

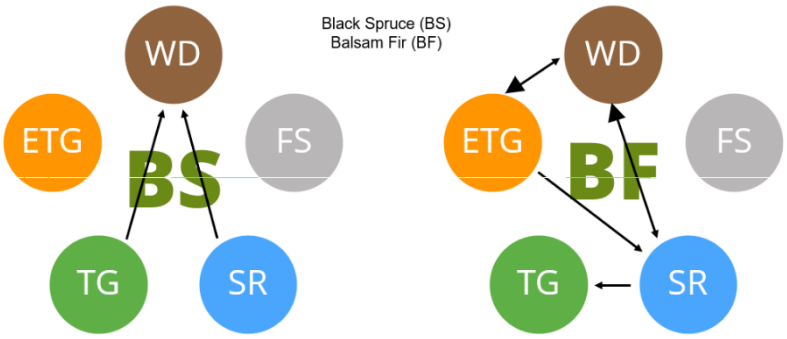

FIGURE 7 : Significant relationships identified by the Granger causality test among phenological periods: Winter Dehydration (WD), Freezing State (FS), Spring Rehydration (SR), Transpiration and Growth (TG) and End of Transpiration and Growth (ETG). The diagram on the left represents causal relationships for black spruce (BS), while on the right diagram shows those for balsam fir (BF). Arrows indicate the direction of influence between periods, and their thickness reflects the strength of the causal relationship detected.

After assessing how events in one period influence subsequent phases over time (FIGURE 7), we used correlation analyses to test whether variation in Seasonal Delta values (FIGURE 6) is associated with the magnitude of the following phase, based on the seasonal amplitudes of the five periods (TABLE 6, FIGURE 8). Most of the phase amplitudes were not correlated between each other (TABLE 6). However, the amplitude of Winter Dehydration phase was correlated with many phases. First, the End Transpiration and Growth negatively influence subsequent Winter Dehydration, in both black spruce (r=0.77) and balsam fir (r=0.81), respectively (TABLE 6, FIGURE 8, TABLE 7), indicating that lower desiccation at the end of the summer, lead to higher dehydration during the autumn. Whereas, more intense Winter Dehydration phase was negatively correlated with the subsequent spring rehydration (r = 0.82) and transpiration and growth (r = 0.87), but only for fir. The years characterized by stronger winter dehydration (i.e. more negative values) were followed by higher stem rehydration and higher stem growth (FIGURE 8) confirming a strong carry-over effect across seasons

for fir (FIGURE 7). In the correlation plots (FIGURE 8), the balsam fir curve places the subsequent years of severe defoliation, 2021 and 2022, at the upper extreme, indicating a lower stem dehydration (less negative) and winter rehydration for those years. A sensitivity analysis excluding these years confirmed that, although they exerted high influence (TABLE 7), they did not generate the observed negative trends.

TABLE 6 : Correlation between the seasonal amplitude (mm) of one phase with the following one in black spruce and in balsam fir.

Period 1	**Period 2**	**Spruce**		**Fir**	
		Corr.	**P-Value**	**Corr.**	**P-Value**
End of Transpiration and Growth	Freezing State	-0.0325	0.9449	-0.3132	0.4940
End of Transpiration and Growth	Spring Rehydration	-0.2738	0.5524	0.5795	0.1727
End of Transpiration and Growth	Transpiration and Growth	0.0403	0.9245	0.6436	0.0851
End of Transpiration and Growth	Winter Dehydration	**-0.7783**	**0.0393**	**-0.8124**	**0.0264**
Freezing State	Spring Rehydration	-0.0468	0.9299	-0.3502	0.4961
Freezing State	Transpiration and Growth	-0.3268	0.4743	-0.3042	0.5070
Freezing State	Winter Dehydration	0.3461	0.4470	0.0766	0.8702
Spring Rehydration	Transpiration and Growth	0.2484	0.5912	0.5279	0.2232
Spring Rehydration	Winter Dehydration	-0.0518	0.9223	**-0.8766**	**0.0219**
Transpiration and Growth	Winter Dehydration	-0.6137	0.1427	**-0.8299**	**0.0208**

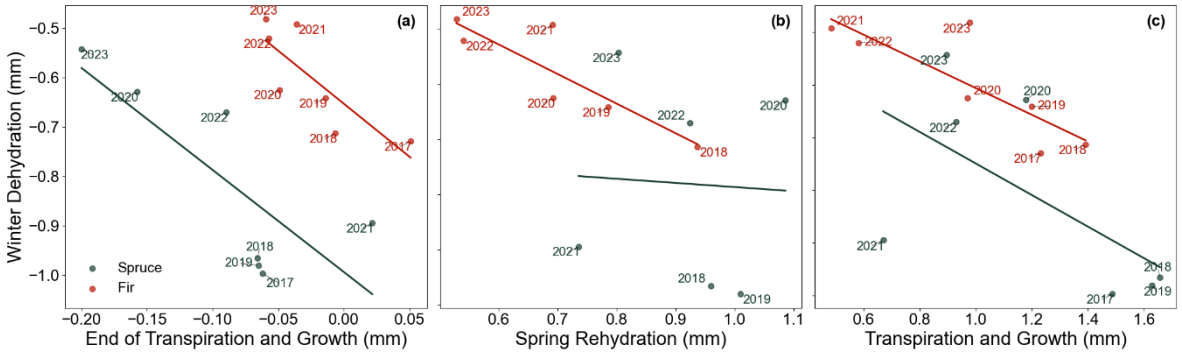

FIGURE 8 : Significant correlations and trends among Seasonal Delta metrics reported in TABLE 6. Scatterplots show the relationships between Winter Dehydration and (a) End of Transpiration and Growth, (b) Spring Rehydration and (c) Transpiration and Growth for spruce and fir, with tear-labeled points ad fitted lines.

TABLE 7 : Correlation diagnostics for period pairs with significant associations. For each pairing, we report Pearson's r (all years), Pearson's r excluding years flagged as extremes in the correlation plots (FIGURE 8), Spearman's ρ, and the robust Theil–Sen slope with 95% confidence intervals.

Period pair	Pearson r (p)	Pearson r without flags (p)	Spearman ρ (p)	Theil-Sen slope	95% CI (Theil-Sen)
Spruce					
Winter Dehydration vs End of Transpiration and Growth	-0.778 (0.0393)	-0.895 (0.0159)	-0.786 (0.0362)	-0.263	[-0.630, -0.050]
Fir					
Winter Dehydration vs End of Transpiration and Growth	-0.812 (0.0264)	-0.784 (0.065)	-0.893 (0.0068)	-2.724	[-9.410, -0.440]
Winter Dehydration vs Spring Rehydration	-0.877 (0.0219)	-0.975 (0.0047)	-0.943 (0.0048)	-1.612	[-5.542, -0.008]
Winter Dehydration vs Transpiration and Growth	-0.830 (0.0209)	-0.964 (0.0020)	-0.750 (0.0522)	-3.111	[-4.762, 0.047]

2.4 WATER-USE STRATEGY AND HYDRAULIC CONTROL

Transpiration was then analysed to determined how it can influence the seasonal stem variation, especially during the period of Transpiration and Growth, when sap flow was measured, and the effect of defoliation. Different patterns were obtained according to species (FIGURE 9). In fir, during the transpiration and growth period, the daily average water use (Qs) influences the amplitude of the transpiration and growth phases ($R^2 = 0.64$; $p<0.001$). In black spruce however, the mean daily

tree water use was independent of the amplitude of stem increment across the years (seasonal delta; R^2 = 0.05) (FIGURE 9). This pattern indicates that stem growth of balsam fir was strongly dependent on the amount of water used, while in black spruce growth appears more decoupled from water use.

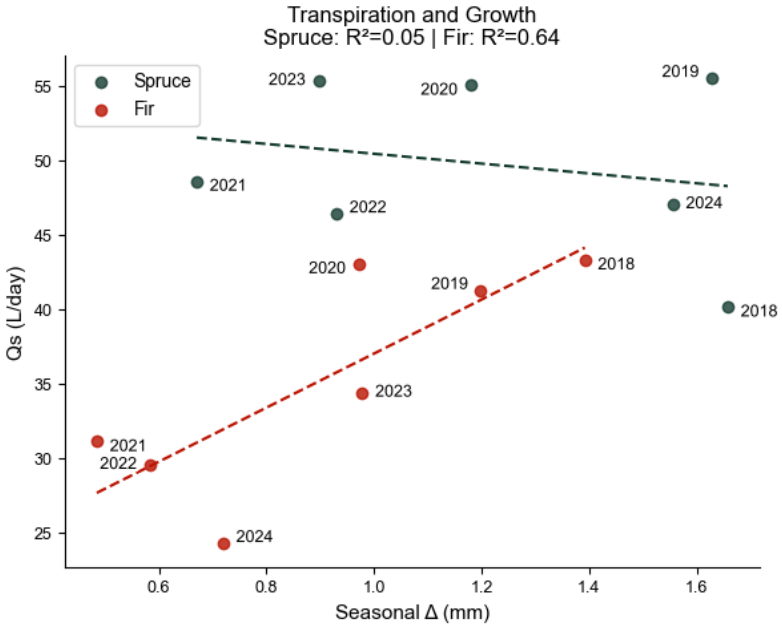

FIGURE 9 : Daily average water use (L·day^{-1}) expressed in function of the amplitude (seasonal Δ) of the Transpiration and Growth period (mm) for balsam fir (in red) and black spruce (in black). The years are indicated in reference.

In both species, tree's water use increased with VPD $\left(\hat{\beta} = 1.795, SE = 0.109, p < 0.001\right)$, meaning that under the reference conditions (black spruce in 2018), higher atmospheric demand (high VPD) promote greater sap flow in trees ($Q_{S;}$ L/day, after back-transformation) (FIGURE 10, FIGURE 11). The significant VPD*Species interaction revealed that fir was less sensitive to increased VPD than black spruce $\left(\hat{\beta} = -0.526, SE = 0.066, p < 0.001\right)$. While the baseline VPD slope for black spruce is 1.795, the slope for balsam fir decreased to approximately 1.269 [1.795 + (-0.526)], suggesting that this species partially restricts transpiration under high evaporative demand. The non-significant main effect of species on the intercept (p = 0.262) indicates that, under reference VPD conditions, both species exhibited similar baseline sap flow rates.

When VPD was held constant at its sample mean, annual contrasts indicated that tree water use declined markedly in 2021 $\left(\hat{\beta} = -1.008, p < 0.001\right)$, 2022 $\left(\hat{\beta} = -1.099, p < 0.001\right)$, and with a

smaller reduction in 2024 $\left(\hat{\beta} = -1.316, p < 0.001\right)$, while in 2023 we observed a small recovery $\left(\hat{\beta} = 0.622, p = 0.007\right)$. These years correspond to the post-defoliation period following the spruce budworm outbreak, when canopy loss likely reduced transpiring leaf area. The year-specific VPD slopes also varied: they were steeper in 2019 $\left(\hat{\beta} = 0.485, p = 0.001\right)$, 2021 $\left(\hat{\beta} = 0.795, p < 0.001\right)$, 2022 $\left(\hat{\beta} = 0.693, p < 0.001\right)$, and 2023 $\left(\hat{\beta} = 0.410, p = 0.002\right)$, whereas 2020 and 2024 showed no significant deviations from the reference slope (p = 0.801 and p = 0.075, respectively). These profiles suggest that interannual modulation of the VPD response was particularly strong in 2019, 2021, and 2022, with more moderate adjustments in 2023–2024.

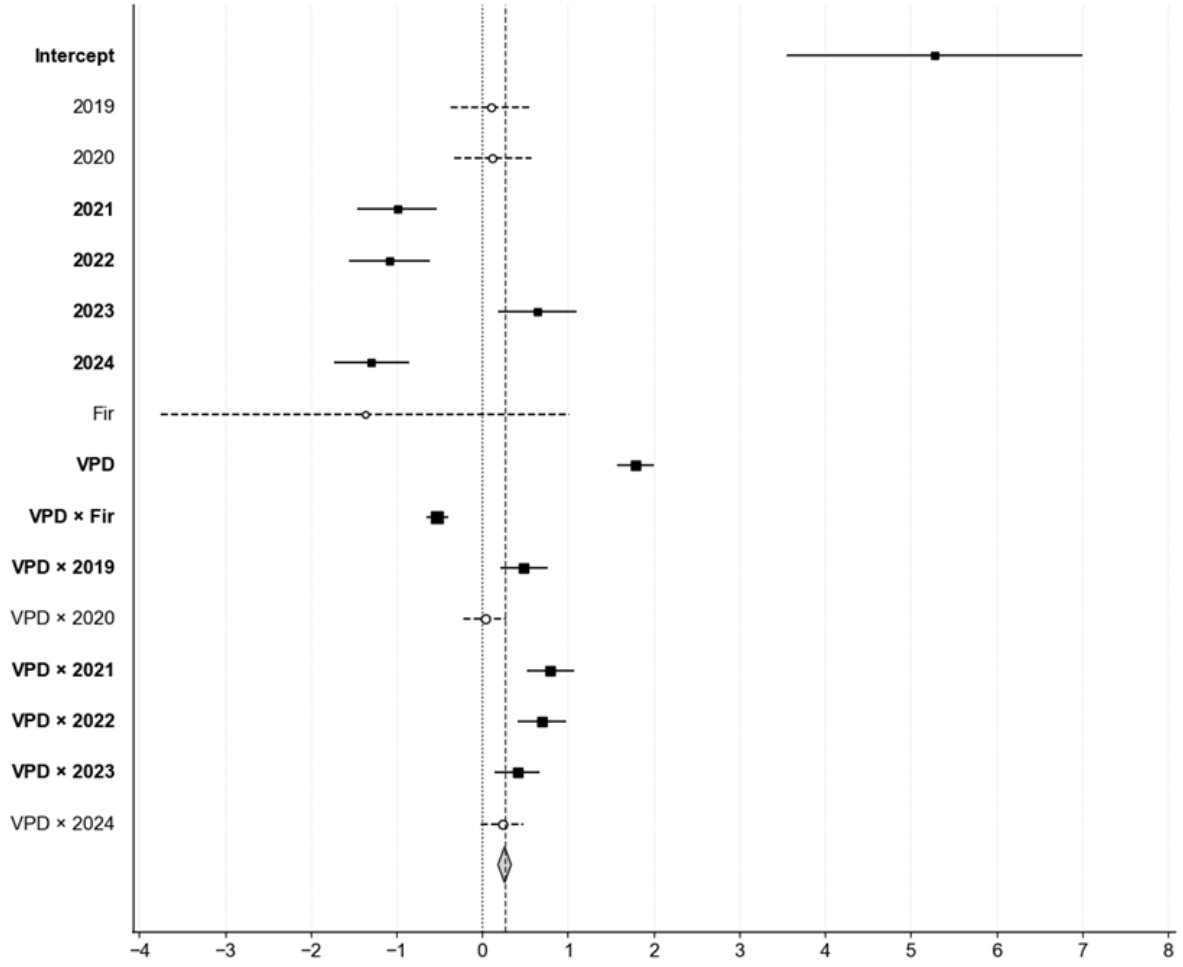

FIGURE 10 : Forest plot of the fixed effects from the mixed-effects model after the Box-Cox transformation of Q_S values. The vertical line at zero indicates the null effect. Markers show point estimates, and horizontal lines their 95% confidence intervals. Black squares indicate significant coefficients, whereas white circles indicate non-significant coefficients; bold labels also denote significant fixed effects. For significant coefficients, square size is proportional to the standard error. The diamond and dashed line represent the combined effect of VPD, with the center showing the variance-weighted mean estimate and the extremities the 95% confidence interval.

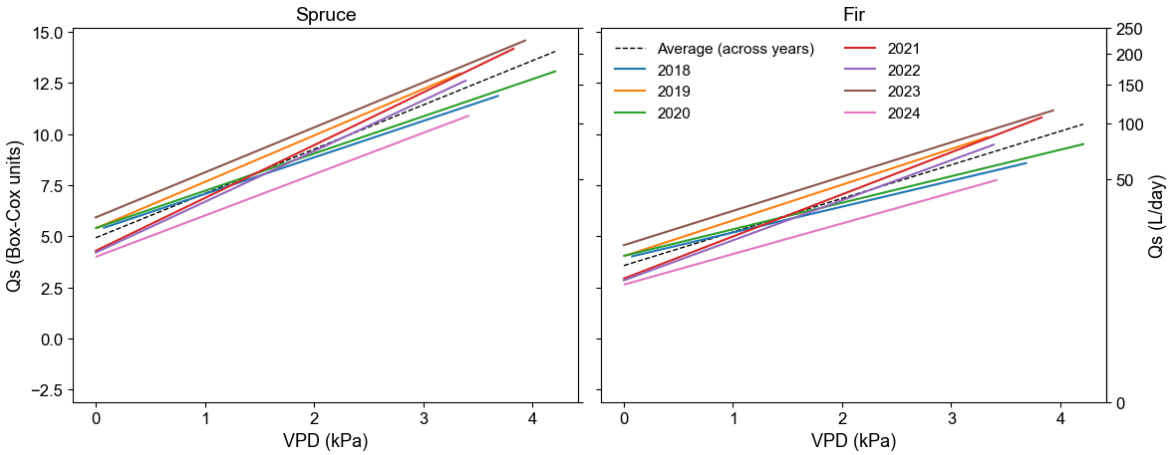

FIGURE 11 : Relationship between water use (Qs, L·day^{-1}) and vapor pressure deficit (VPD) expressed by year for black spruce and balsam fir. Colored lines represent year-specific slopes from the linear mixed-effects model (FIGURE 10) in the Box–Cox scale, plotted over the observed range of VPD each year. Faded points show individual observations. The dashed black line indicates the average slope across years. The left y-axis shows Qs in Box–Cox units, while the right y-axis shows the corresponding back-transformed values in L·day^{-1}.

The comparison between observed and predicted means (FIGURE 12) indicates that the model adequately captures the temporal variability in Qs, reproducing both the peaks in 2019 and 2023 and the lower levels observed in 2021–2022 and 2024, with realistic uncertainty bands.

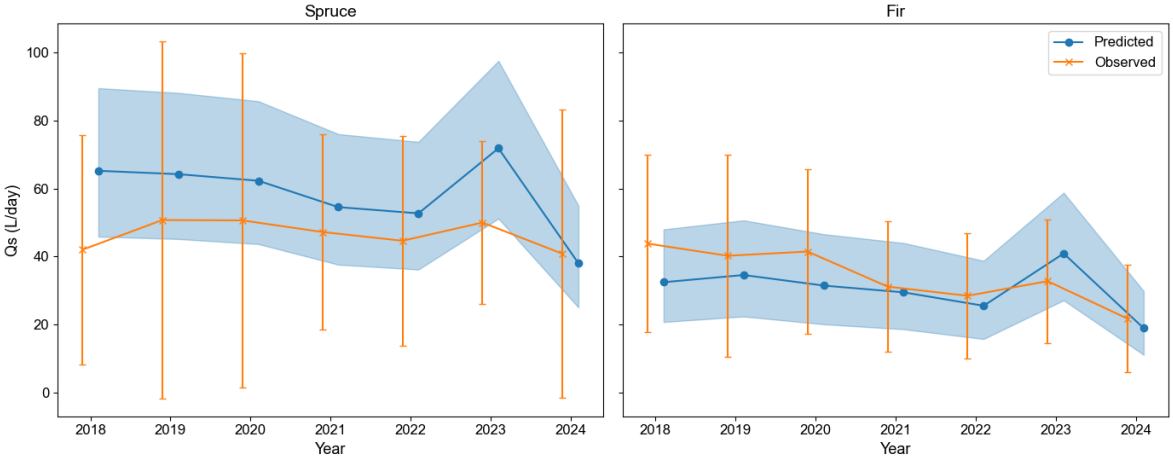

FIGURE 12 : Observed vs. predicted Qs (L/day, after Box-Cox back-transformation) by year for spruce and fir. The blue line shows mean predicted by the linear mixed-effects model evaluated at the mean VPD with shaded 95% confidence intervals. The orange line represents observed means with standard-deviation error bars, and a small horizontal jitter (±0.1) is applied to reduce overlap.

CHAPITRE 3
DISCUSSION

3.1 IMMEDIATE AND CUMULATIVE IMPACT OF SPRUCE BUDWORM ON RADIAL GROWTH DURING THE TRANSPIRATION AND GROWTH PHASE AND STEM WINTER SHRINKAGE

There were clear differences both between species and across years (intra-annual variation) in phenological phases and in the physiological strategies employed to cope with environmental and biological stress induced by spruce budworm defoliation. Following 2020, when the defoliation index (DI) peaked at 3 (between 70%-100% of new foliage damage (MRNF 2023)), both species showed a general reduction in the amplitudes of most seasonal stem radius variation phases compared with the mean of the years preceding the outbreak. This physiological suppression was most pronounced in the growth period. Notably, in 2021 and 2022, the years immediately following the severe spruce budworm defoliation event, balsam fir exhibited the lowest amplitude in transpiration and growth (mm) and, consequently, the lowest seasonal transpiration, with mean daily water use of ~30 $L \cdot day^{-1}$ (Qs). These findings align with tree-ring growth results indicating that the most negative impact on radial increment typically occurs with a lag of one to four years after defoliation (Pothier *et al.* 2005; Fierravanti *et al.* 2015; MacLean *et al.* 2024), thereby supporting the presence of delayed negative lag effects of spruce budworm, not only on radial growth but also on water exchange with the atmosphere.

The delayed impacts on sap flow (a proxy of transpiration) and radial growth were likely caused by loss of photosynthetic area and reduced new xylem production during the growing season, which directly limits the tree's maximum sap flow capacity in the following years. First, spruce budworm-induced defoliation disrupts carbon allocation patterns, leading to starch depletion in both needle and stem wood and causing a drastic reduction in radial growth rates (Fierravanti et al. 2019; Deslauriers et al. 2023). Additional evidence suggests that carbon allocation to ectomycorrhiza also declines in response to defoliation (Kolb *et al.* 1999). Second, suppressed growth due to a deceleration in new xylem formation increases hydraulic resistance (Axelson *et al.* 2014; Schäfer *et*

al. 2014), which may further reduce maximum sap flow capacity, as observed in our study. Spruce budworm outbreaks modify cellular characteristics in latewood cells, reducing the number of tracheid formed and altering anatomical features, including lumen area and cell-wall thickness, which decreases wood density and increases vulnerability to cavitation (Paixao *et al.* 2019; Devautour 2025). Following defoliation, host species engage in a preferential reallocation of carbon (MacLean 2016; MacLean *et al.* 2024), moving resources to buds and shoots to restore photosynthetic capacity through primary growth at the expense of secondary growth (Deslauriers *et al.* 2019).

The winter dehydration phase is characterized by maximum radial stem contraction and reflects a whole-tree cold-season stress response involving needles, bark, and trunk. In a related context, Delapierre *et al.* (2024) reported winter stem contraction ranging from 0.03 to 1.478 mm in *Picea abies* (L.) H. Karst. Using our sign convention (negative values indicate shrinkage), we observed winter shrinkage of 0.48–0.73 mm in balsam fir and 0.54–1.00 mm in black spruce. When soils and stem tissues are frozen, water uptake is constrained while evergreen canopies can still lose water under high atmospheric demand (i.e., “frost drought”), creating a hydraulic imbalance expressed as progressive stem shrinkage (Mayr *et al.* 2006; Sevanto *et al.* 2006; Delapierre *et al.* 2024). At the stem level, freeze–thaw dynamics and extracellular freezing promote water redistribution out of cells toward apoplastic ice, lowering turgor and causing tissue contraction (Zweifel et Häsler 2000); consequently, winter diameter changes are often dominated by bark water content and related hygroscopic effects (Oberhuber *et al.* 2020; Delapierre *et al.* 2023). By extending the observation that defoliation can improve tree water status by reducing canopy transpiration (Balducci *et al.* 2020), we propose that spruce budworm-driven reductions in needle area may lower the tension transmitted to frozen basal sections in winter, limiting dehydration-driven shrinkage. In black spruce, this is consistent with evidence that defoliation can conserve internal stem water (Bouzidi *et al.* 2019) and with reports that black spruce sustains lower defoliation than other host species, factors that combined would reduce cumulative winter desiccation risk (Wu *et al.* 2020).

3.2 PHENOLOGICAL COUPLING BETWEEN PHASES AND INTERNAL VULNERABILITY TO SPRUCE BUDWORM DEFOLIATION

The temporal relationship whereby an event in one period influences subsequent phases is central to understanding phenological coupling and future tree vulnerability. The Granger test assessed whether earlier phases could predict stem radius variation in later periods, while correlation analyses quantified how phase amplitudes co-vary. We found that Spring Rehydration and Transpiration and Growth amplitudes can predict subsequent Winter Dehydration; however, a negative correlation emerged only at the end of the growth period. Because black spruce exhibits few significant causal relationships between seasonal phases, even after years of accumulating defoliation, this pattern points to a conservative and highly regulated physiological strategy for buffering against stress (Balducci *et al.* 2021a). The absence of interannual carry-over effects suggests greater stability, as the physiological magnitude of a given phase does not constrain the tree's capacity to recover in the subsequent phase of the following year; it may also indicate lower defoliation levels in black spruce, given that balsam fir is the preferred host and defoliation pressure is often higher on fir than on spruce (Nealis et Régnière 2004).

On the other hand, in balsam fir, the Granger results indicate a stronger and more temporally structured relationship among phases. These results highlight that balsam fir shows tighter physiological coupling among its annual phases and potential physiological impacts of spruce budworm. The argument supporting this statement relies on two possible mechanisms: (i) a consistent lag effect (internal memory), whereby a reduction in transpiration and growth amplitude negatively constrains the magnitude of the next year's stem rehydration and transpiration and growth (Pothier *et al.* 2005; Fierravanti *et al.* 2015; MacLean *et al.* 2024); and (ii) defoliation causes a loss of photosynthetic capacity, leading to reduced Carbon-Hydraulic debits and depletion of non-structural carbohydrate reserves (i.e., starch and sucrose depletion) (Deslauriers *et al.* 2015; Fierravanti *et al.* 2019; Deslauriers *et al.* 2025), which may impair the tree's ability to recover turgor during spring rehydration in the following year, primarily because depleted sucrose limits the carbon supply required for osmotic adjustment and refilling processes (Mayr *et al.* 2014; Deslauriers *et al.* 2025). This process

may also impair carbon mobilization for growth during the subsequent transpiration and growth period, thereby increasing the negative net effect on carbon storage.

3.3 DIVERGENT SPRUCE BUDWORM EFFECT IN WATER-USE STRATEGY AND HYDRAULIC CONTROL

We further demonstrated that balsam fir exhibits growth closely coordinated with tree water use, whereas black spruce experiences relatively high-water loss even during periods of limited growth. The defoliation-induced reduction in tree water-use capacity suggests that balsam fir is highly susceptible to leaf area loss caused by spruce budworm (Hennigar *et al.* 2008; Salmon *et al.* 2015; Paixao *et al.* 2019; Balducci *et al.* 2020; Deslauriers *et al.* 2023). In contrast, black spruce appears to adopt a more hydraulically decoupled strategy, which may reflect reduced water-use efficiency (Bouzidi *et al.* 2019). This less conservative response to defoliation (e.g., maintaining high sap flow rates even during periods of minimal radial growth) may indicate greater hydraulic stability under stress (Bouzidi *et al.* 2019; Pappas *et al.* 2020).

Interestingly, this reduction in water use was primarily caused by spruce budworm defoliation across years, rather than by interannual variability in VPD, and it was stronger in balsam fir than in black spruce (Balducci *et al.* 2020; Oogathoo *et al.* 2020; Deslauriers *et al.* 2023). This pattern suggests that balsam fir is less hydraulically resilient in compensating for leaf loss caused by spruce budworm defoliation compared with black spruce (Delzon *et al.* 2010; Salmon *et al.* 2015). In fact, fir has an inherently lower Qs capacity than spruce (FIGURE 10; reduced intercept) and higher sensitivity of canopy conductance (FIGURE 10; using the steeper slope than spruce as a proxy; (Oren *et al.* 1999; Brodribb et Jordan 2008; Balducci *et al.* 2020; Oogathoo *et al.* 2020; Devautour 2025)). In black spruce, as observed by Bouzidi *et al.* (2019) in saplings, reduced leaf area helped conserve internal stem water, avoiding large decreases in shoot water potential. This supports the hypothesis that defoliation can improve post-stress water relations because reduced leaf area shifts the water balance, potentially increasing leaf-specific conductance and transpiration per unit leaf area. We suggest that because balsam fir, the primary host of spruce budworm (Blais 1958; Hennigar *et al.*

2008; Balducci *et al.* 2021a), exhibits a greater growth reduction under spruce budworm defoliation than black spruce, part of its post-outbreak limitation may reflect structural constraints on wood formation (Campbell *et al.* 2008; Deslauriers *et al.* 2015). Furthermore, following spruce budworm attack, both balsam fir and black spruce tend to redirect carbon investment toward bud development at the expense of secondary stem growth and the production of new tracheid (Deslauriers *et al.* 2019). In line with this interpretation, spruce budworm defoliation has been associated with a decline in annual radial growth and with modifications in latewood anatomy, specifically a reduction in cell-wall thickness and a shift in the lumen-to-wall ratio (Paixao *et al.* 2019; Devautour 2025), which can translate into shifts in wood density and wood quality (Paixao *et al.* 2019). These changes may also include a lower proportion of latewood within the growth ring (Axelson *et al.* 2014). Although conifer wood density is a heritable trait under significant genetic control (Nabais *et al.* 2018), it remains highly sensitive to variation in environmental conditions because its physical expression depends largely on tracheid structural characteristics (Rathgeber 2017; Devautour 2025).

Therefore, new xylem production may be constrained by defoliation-driven growth reductions, potentially through a decrease in the conduit area formed during defoliated years, as xylem traits can be altered during defoliation via three main pathways: (1) reduced tree water status (Salmon *et al.* 2015; Bouzidi *et al.* 2019; Balducci *et al.* 2020), (2) diminished carbon reserves (Fierravanti *et al.* 2019; Deslauriers *et al.* 2023), and (3) partitioning of carbon investment between apical bud development and secondary stem growth (Deslauriers *et al.* 2019). Consistent with this mechanism, after three consecutive years of defoliation, both balsam fir and black spruce showed reduced lumen area and altered cell-wall traits (Paixao *et al.* 2019). This suggests that three consecutive years of defoliation affected the water-conducting capacity of the xylem (reduced lumen), and the increase in wood density was likely due to a change in the ratio of cell walls to lumen. Narrower ring widths together with fewer latewood tracheid were observed after three years in balsam fir and four years in black spruce; overall, these responses were associated with lower wood density (Krause et Morin 1995; Hennigar *et al.* 2008; Paixao *et al.* 2019; Devautour 2025). These anatomical modifications reflect a carbon-saving strategy that prioritizes primary growth at the expense of the mechanical

stability and hydraulic security, specifically resistance to tracheid implosion and cavitation, typically provided by latewood (Deslauriers *et al.* 2015; Rathgeber 2017; Paixao *et al.* 2019; Devautour 2025).

This structural compromise, combined with the evident lag in subsequent years in balsam fir could be caused by reduced hydraulic efficiency and canopy conductance and, therefore, a lower maximum Qs capacity in balsam fir compared with black spruce (Balducci *et al.* 2020; Oogathoo *et al.* 2020). Furthermore, given the strong decoupling between tree growth and transpiration in black spruce (Pappas *et al.* 2020), it appears that long-term water-use efficiency is reduced during spruce budworm outbreak years. This suggests that remaining foliage in black spruce can sustain basic carbon fixation and physiological functions without undergoing the subsequent hydraulic collapse observed in balsam fir (Salmon *et al.* 2015; Balducci *et al.* 2020). For black spruce, this strategy acts as a buffer, preventing the negative feedback loop that balsam fir experiences and reinforcing black spruce's superior resilience. Indeed, defoliation in black spruce reduces leaf area, which helps the tree conserve stem water and improves its water status post-stress (Bouzidi et al. 2019), allowing it to sustain higher water use despite reduced radial growth (Pappas *et al.* 2020; Balducci *et al.* 2021a). In contrast, water use and growth are more tightly coordinated in balsam fir, which may require a compensatory mechanism to increase water-use efficiency while growth declines (Simard *et al.* 2012; Deslauriers *et al.* 2023). Evidence from tree-ring stable isotopes demonstrates that defoliated balsam fir exhibits a significant enrichment of $\delta^{13}C$ in wood cellulose (Simard et al. 2012). While this is often an indicator of increased water-use efficiency, Simard et al. (2012) suggest this enrichment likely results from the mobilization of stored 13C-enriched carbohydrates to compensate for the loss of photosynthetic needles, as direct photosynthetic compensation is frequently absent or limited in mature trees and certain field studies (Lavigne *et al.* 2001; Simard *et al.* 2012). Supporting this, stem starch depletion is a primary physiological response during spruce budworm outbreaks (Deslauriers et al. 2023).

CONCLUSION

This study developed and applied time-series analytical method to quantify sap flow (Qs, $L \cdot day^{-1}$) and stem radius variation (mm) in black spruce and balsam fir. The goal was to clarify how spruce budworm outbreaks alters tree physiology across successive seasonal phases (winter dehydration, freezing state, spring rehydration, and transpiration and growth) over an eight-year period. Overall, our results show that spruce budworm impacts are not confined to the period when defoliation occurs, but propagate across the annual physiological cycle, with responses that differ markedly between species and among years.

Consistent with our first hypothesis, years characterized by active spruce budworm defoliation were associated with reduced physiological performance, expressed as diminished water use (Qs, $L \cdot day^{-1}$) and constrained radial dynamics (stem radius variation). Importantly, these impacts were not restricted to the transpiration and growth period; rather, we observed lagged, negative carryover effects on tree productivity that persisted into subsequent years and across other important seasonal phases. The time-series framework further indicated that defoliation effect can reorganize intra-annual physiological dynamics by altering transitions among dehydration, freezing, rehydration, and growth. This temporal carryover shaped species-specific vulnerability: balsam fir exhibited tighter phenological coupling and stronger cross-phase dependencies than black spruce. This suggests that stress in one seasonal window constrains subsequent physiological states. Meanwhile, black spruce showed fewer cross-phase causal links even under cumulative defoliation, consistent with a more conservative and regulated strategy that limits stress propagation.

Regarding our second hypothesis, climatic forcing, captured by VPD, emerged as a key modulator of tree water use, interacting with outbreak context and species strategy. Under defoliation pressure, elevated evaporative demand (i.e. VPD) is expected to intensify hydraulic constraints. Our time-series analyses support this joint interpretation, indicating that high VPD can amplify reductions in transpiration and associated radial dynamics, particularly in the more physiologically vulnerable species. These results underscore that spruce budworm-driven responses cannot be interpreted independently of concurrent atmospheric demand, and that the magnitude and persistence of outbreak impacts are embedded within broader hydroclimatic stress conditions.

In summary, this study demonstrates that spruce budworm outbreaks generate both immediate and lagged impacts on conifer physiology and that these impacts are mediated by seasonal phase coupling and species-specific hydraulic regulation. balsam fir shows stronger cross-phase carryover, tighter coupling between water use and growth, and lower capacity to buffer leaf loss, whereas black spruce exhibits a more conservative strategy that limits the propagation of stress across seasons and maintains water use even when growth is constrained. Beyond these ecological insights, the time-series analytical approach developed here provides a transferable framework for monitoring tree function through outbreaks and climatic variability, improving our capacity to detect vulnerability and resilience in boreal forests experiencing interacting biotic and abiotic stressors.

LISTE DE RÉFÉRENCES

Améglio T, Cochard H et Ewers FW. 2001. Stem diameter variations and cold hardiness in walnut trees. Journal of Experimental Botany, 52 : 2135-2142.

Axelson JN, Bast A, Alfaro R, Smith DJ et Gärtner H. 2014. Variation in wood anatomical structure of Douglas-fir defoliated by the western spruce budworm: a case study in the coastal-transitional zone of British Columbia, Canada. Trees, 28 : 1837-1846.

Balducci L, Rozenberg P et Deslauriers A. 2021a. Variation of stem radius in response to defoliation in boreal conifers. Frontiers in Forests and Global Change, 4.

Balducci L, Fierravanti A, Rossi S, Delzon S, De Grandpré L, Kneeshaw DD et Deslauriers A. 2020. The paradox of defoliation: Declining tree water status with increasing soil water content. Agricultural and Forest Meteorology, 290 : 108025.

Balducci L, Deslauriers A, De Barba D, Rossi S, Houle D, Bergeron Y et Morin H. 2021b. Influence of soil warming and N-addition on sap flux density and stem radius variation in boreal stands in Quebec, Canada. Ecohydrology, 14 : e2261.

Blais JR. 1952. The relationship of the spruce budworm (*Choristoneura fumiferana*, Clem.) to the flowering condition of balsam fir (*Abies balsamea* (L.) Mill.). Canadian Journal of Zoology, 30 : 1-29.

Blais JR. 1958. The vulnerability of balsam fir to spruce budworm attack in northwestern Ontario, with special reference to the physiological age of the tree. The Forestry Chronicle, 34 : 405-422.

Bond-Lamberty B, Wang C et Gower ST. 2002. Aboveground and belowground biomass and sapwood area allometric equations for six boreal tree species of northern Manitoba. Canadian Journal of Forest Research, 32 : 1441-1450.

Bouzidi HA, Balducci L, Mackay J et Deslauriers A. 2019. Interactive effects of defoliation and water deficit on growth, water status, and mortality of black spruce (*Picea mariana* (Mill.) B.S.P.). Annals of Forest Science, 76 : 21.

Brodribb TJ et Jordan GJ. 2008. Internal coordination between hydraulics and stomatal control in leaves. Plant, Cell & Environment, 31 : 1557-1564.

Burton PJ, Bergeron Y, Bogdanski BEC, Juday GP, Kuuluvainen T, McAfee BJ, Ogden A, Teplyakov VK, Alfaro RI, Francis DA, Gauthier S et Hantula J. 2010. Sustainability of boreal forests and forestry in a changing environment. IUFRO World Series, 25 : 249–282.

Campbell EM, MacLean DA et Bergeron Y. 2008. The severity of budworm-caused growth reductions in balsam fir/spruce stands varies with the hardwood content of surrounding forest landscapes. Forest Science, 54 : 195-205.

Canadian Forest Service. 2025. The State of Canada’s Forests: Annual Report 2025. 116 p.

De Swaef T, De Schepper V, Vandegehuchte MW et Steppe K. 2015. Stem diameter variations as a versatile research tool in ecophysiology. Tree Physiology, 35 : 1047-1061.

Delapierre F, Fonti P, Lischke H et Moos C. 2023. A method to quantify and account for the hygroscopic effect in stem diameter variations. Frontiers in Forests and Global Change, Volume 6 - 2023.

Delapierre F, Moos C, Lischke H et Fonti P. 2024. Signs of frost drought in stem diameter variations. Agricultural and Forest Meteorology, 358 : 110247.

Delzon S, Douthe C, Sala A et Cochard H. 2010. Mechanism of water-stress induced cavitation in conifers: bordered pit structure and function support the hypothesis of seal capillary-seeding. Plant, Cell & Environment, 33 : 2101-2111.

Deslauriers A, Rossi S et Anfodillo T. 2007. Dendrometer and intra-annual tree growth: What kind of information can be inferred? Dendrochronologia, 25 : 113-124.

Deslauriers A, Caron L et Rossi S. 2015. Carbon allocation during defoliation: testing a defense-growth trade-off in balsam fir. Frontiers in Plant Science, 6 : 338.

Deslauriers A, Morin H, Urbinati C et Carrer M. 2003. Daily weather response of balsam fir (*Abies balsamea* (L.) Mill.) stem radius increment from dendrometer analysis in the boreal forests of Québec (Canada). Trees, 17 : 477-484.

Deslauriers A, Fournier M-P, Cartenì F et Mackay J. 2019. Phenological shifts in conifer species stressed by spruce budworm defoliation. Tree Physiology, 39 : 590-605.

Deslauriers A, Balducci L, Fierravanti A et Bouchard M. 2023. Changes in water status and carbon allocation in conifers subjected to spruce budworm defoliation and consequences for tree mortality and forest management. Dans : Girona MM*, et al.* éds. Boreal Forests in the Face of Climate Change: Sustainable Management. Springer International Publishing, Cham, p. 249-269.

Deslauriers A, Benoit P, Balducci L, Néron V, Guzmán-Marín R, Rossi S, Lavoie S et Isabel N. 2025. The effects of metabolic and functional traits on bud opening: Comparing warming and defoliation in conifers. Plant Physiology, 199.

Devautour C. 2025. Comment la défoliation de la tordeuse des bourgeons de l'épinette façonne-t-elle les traits hydrauliques et anatomiques des conifères boréaux ? , Université du Québec à Chicoutimi, Chicoutimi, 66 p.

Direction de la Protection des Forêts. 2025 (mis à jour le 05 fevrier 2025). Natural disturbance data - Insect: Spruce budworm. Consulté le 07 mars 2025, https://open.canada.ca/data/en/dataset/fbf12500-bffe-4209-a1ae-fba86f154ebf

Dusart N, Moulia B, Saudreau M, Serre C, Charrier G et Hartmann FP. 2024. Differential warming at crown scale impacts walnut primary growth onset and secondary growth rate. Journal of Experimental Botany, 75 : 7127-7144.

Dymond CC, Neilson ET, Stinson G, Porter K, MacLean DA, Gray DR, Campagna M et Kurz WA. 2010. Future spruce budworm outbreak may create a carbon source in eastern canadian forests. Ecosystems, 13 : 917-931.

Environment and Natural Resources. 2024 (mis à jour le 01 octobre 2024). Canadian climate normals 1991-2020 data. Consulté le 21 janvier 2025, https://climate.weather.gc.ca/climate_normals/results_1991_2020_e.html?searchType=stnProv&lstProvince=QC&txtCentralLatMin=0&txtCentralLatSec=0&txtCentralLongMin=0&txtCentralLongSec=0&stnID=83000000&dispBack=0

FAO. 2020. Global forest resources assessment 2020—Key findings. Rome, p. 16.

Fierravanti A, Rossi S, Kneeshaw D, De Grandpré L et Deslauriers A. 2019. Low non-structural carbon accumulation in spring reduces growth and increases mortality in conifers defoliated by spruce budworm. Frontiers in Forests and Global Change, Volume 2 - 2019.

Fierravanti A, Cocozza C, Palombo C, Rossi S, Deslauriers A et Tognetti R. 2015. Environmental-mediated relationships between tree growth of black spruce and abundance of spruce budworm along a latitudinal transect in Quebec, Canada. Agricultural and Forest Meteorology, 213 : 53-63.

Fortin M, Lavoie J-F, Régnière J et Saint-Amant R. 2022. A Web API for weather generation and pest development simulation in North America. Environmental Modelling & Software, 157 : 105476.

Granger CWJ. 1969. Investigating causal relations by econometric models and cross-spectral methods. Econometrica, 37 : 424-438.

Granier A. 1985. Une nouvelle méthode pour la mesure du flux de sève brute dans le tronc des arbres. Annals of Forest Science, 42 : 193-200.

Granier A. 1987. Evaluation of transpiration in a Douglas-fir stand by means of sap flow measurements. Tree Physiology, 3 : 309-320.

Grüning MM, Simon J, Rennenberg H et A LM-A. 2017. Defoliating insect mass outbreak affects soil N fluxes and tree N nutrition in scots pine forests. Frontiers in Plant Science, 8 : 954.

Hennigar CR, MacLean DA, Quiring DT et Kershaw JA, Jr. 2008. Differences in spruce budworm defoliation among balsam fir and white, red, and black spruce. Forest Science, 54 : 158-166.

Huang J-G, Deslauriers A et Rossi S. 2014. Xylem formation can be modeled statistically as a function of primary growth and cambium activity. New Phytologist, 203 : 831-841.

Kolb TE, Dodds KA et Clancy KM. 1999. Effect of western spruce budworm defoliation on the physiology and growth of potted douglas-fir seedlings. Forest Science, 45 : 280-291.

Koller CN et Leonard DE. 1981. Comparison of energy budgets for spruce budworm *Choristoneura fumiferana* (Clemens) on balsam fir and white spruce. Oecologia, 49 : 14-20.

Köstner B, Falge E et Alsheimer M. 2017. Sap flow measurements. Dans : Foken T éd. Energy and matter fluxes of a spruce forest ecosystem. Springer, Bayreuth, p. 99-112.

Krause C et Morin H. 1995. Impact of spruce budworm defoliation on the number of latewood tracheids in balsam fir and black spruce. Canadian Journal of Forest Research, 25 : 2029-2034.

Lavigne MB, Little CHA et Major JE. 2001. Increasing the sink:source balance enhances photosynthetic rate of 1-year-old balsam fir foliage by increasing allocation of mineral nutrients. Tree Physiology, 21 : 417-426.

Liu Z, Peng C, De Grandpré L, Candau J-N, Work T, Huang C et Kneeshaw D. 2019. Simulation and analysis of the effect of a spruce budworm outbreak on carbon dynamics in boreal forests of Quebec. Ecosystems, 22 : 1838-1851.

MacLean DA. 1980. Vulnerability of fir-spruce stands during uncontrolled spruce budworm outbreaks: A review and discussion. The Forestry Chronicle, 56 : 213-221.

MacLean DA. 2016. Impacts of insect outbreaks on tree mortality, productivity, and stand development. The Canadian Entomologist, 148 : S138-S159.

MacLean DA et Ostaff DP. 1989. Patterns of balsam fir mortality caused by an uncontrolled spruce budworm outbreak. Canadian Journal of Forest Research, 19 : 1087-1095.

MacLean DA, Collier J, MacKinnon WE et Porter KB. 2024. Defoliation level interacts with tree species and soil richness to determine volume increment reduction and recovery from simulated spruce budworm attack. Canadian Journal of Forest Research, 54 : 1155-1169.

Mayr S, Hacke U, Schmid P, Schwienbacher F et Gruber A. 2006. Frost drought in conifers at the alpine timberline: Xylem dysfunction and adaptations. Ecology, 87 : 3175-3185.

Mayr S, Schmid P, Laur J, Rosner S, Charra-Vaskou K, Dämon B et Hacke UG. 2014. Uptake of Water via Branches Helps Timberline Conifers Refill Embolized Xylem in Late Winter Plant Physiology, 164 : 1731-1740.

Ministère des ressources naturelles et des forêts. 2023. Plan d'aménagement spécial pour la récupération des bois touchés par la tordeuse des bourgeons de l'épinette applicable en 2025-2026. Région Saguenay-Lac-Saint-Jean. Unité d'aménagement 027-51. Ministère des ressources naturelles et des forêts, Québec.

Ministère des ressources naturelles et des forêts. 2025. Insectes, maladies et feux dans les fôrets du Québec en 2024. Québec, 73 p.

Morin H. 1994. Dynamics of balsam fir forests in relation to spruce budworm outbreaks in the Boreal Zone of Quebec. Canadian Journal of Forest Research, 24 : 730-741.

Nabais C, Hansen JK, David-Schwartz R, Klisz M, López R et Rozenberg P. 2018. The effect of climate on wood density: What provenance trials tell us? Forest Ecology and Management, 408 : 148-156.

Natural Resources Canada. 2024 (mis à jour le 2025-11-03). Boreal forest. Consulté le 2026-01-21, https://natural-resources.canada.ca/forest-forestry/sustainable-forest-management/boreal-forest

Nealis VG et Régnière J. 2004. Insect-host relationships influencing disturbance by the spruce budworm in a boreal mixedwood forest. Canadian Journal of Forest Research, 34 : 1870-1882.

Niu F, Röll A, Hardanto A, Meijide A, Köhler M, Hendrayanto et Hölscher D. 2015. Oil palm water use: calibration of a sap flux method and a field measurement scheme. Tree Physiology, 35 : 563-573.

Oberhuber W, Sehrt M et Kitz F. 2020. Hygroscopic properties of thin dead outer bark layers strongly influence stem diameter variations on short and long time scales in Scots pine (*Pinus sylvestris* L.). Agricultural and Forest Meteorology, 290 : 108026.

Oogathoo S, Houle D, Duchesne L et Kneeshaw D. 2020. Vapour pressure deficit and solar radiation are the major drivers of transpiration of balsam fir and black spruce tree species in humid boreal regions, even during a short-term drought. Agricultural and Forest Meteorology, 291 : 108063.

Oogathoo S, Duchesne L, Houle D, Kneeshaw D et Bélanger N. 2023. Seasonal, monthly, daily, and diel growth, and water status dynamics of balsam fir in a cold and humid boreal environment. Forests, 14 : 802.

Oren R, Sperry JS, Katul GG, Pataki DE, Ewers BE, Phillips N et Schäfer KVR. 1999. Survey and synthesis of intra- and interspecific variation in stomatal sensitivity to vapour pressure deficit. Plant, Cell & Environment, 22 : 1515-1526.

Paixao C, Krause C, Morin H et Achim A. 2019. Wood quality of black spruce and balsam fir trees defoliated by spruce budworm: A case study in the boreal forest of Quebec, Canada. Forest Ecology and Management, 437 : 201-210.

Pandeya B, Girardin MP, Waldron K, Boucher D, Kneeshaw D et Deslauriers A. 2026. Early growth decline and vegetation change predict black spruce mortality following spruce budworm outbreaks. Ecological Indicators, 183 : 114620.

Pappas C, Maillet J, Rakowski S, Baltzer JL, Barr AG, Black TA, Fatichi S, Laroque CP, Matheny AM, Roy A, Sonnentag O et Zha T. 2020. Aboveground tree growth is a minor and decoupled fraction of boreal forest carbon input. Agricultural and Forest Meteorology, 290 : 108030.

Piene H. 1980. Effects of insect defoliation on growth and foliar nutrients of young balsam fir. Forest Science, 26 : 665-673.

Pothier D, Mailly D et Tremblay S. 2005. Predicting balsam fir growth reduction caused by spruce budworm using large-scale historical records of defoliation. Annals of Forest Science, 62 : 261-267.

Pothier D, Elie J-G, Auger I, Mailly D et Gaudreault M. 2012. Spruce Budworm-Caused Mortality to Balsam Fir and Black Spruce in Pure and Mixed Conifer Stands. Forest Science, 58 : 24-33.

Rathgeber CBK. 2017. Conifer tree-ring density inter-annual variability – anatomical, physiological and environmental determinants. New Phytologist, 216 : 621-625.

Régnière J, Lysyk TJ et Auger M. 1989. Population density estimation of spruce budworm, *Choristoneura fumiferana* (Clem.) (lepidoptera: Tortricidae) on balsam fir and white spruce from 45-cm mid-crown branch tips. The Canadian Entomologist, 121 : 267-281.

Rossi S et Bousquet J. 2014. The bud break process and its variation among local populations of boreal black spruce. Frontiers in Plant Science, Volume 5 - 2014.

Salmon Y, Torres-Ruiz JM, Poyatos R, Martinez-Vilalta J, Meir P, Cochard H et Mencuccini M. 2015. Balancing the risks of hydraulic failure and carbon starvation: a twig scale analysis in declining Scots pine. Plant, Cell & Environment, 38 : 2575-2588.

Saucier J-P, Grondin P, Robitaille A, Gosselin J, Morneau C, Richard P, Brisson J, Sirois L, Leduc A, Morin H, Thiffault E, Gauthier S, Lavoie C et Payette S. 2009. Écologie forestière. Dans : Ordre des ingénieurs forestiers du Québec éd. Manuel de foresterie. Éditions MultiMondes, Québec, QC, Canada, p. 167-315.

Schäfer KVR, Renninger HJ, Clark KL et Medvigy D. 2014. Hydrological responses to defoliation and drought of an upland oak/pine forest. Hydrological Processes, 28 : 6113-6123.

Seabold S et Perktold J. 2010. Statsmodels: Econometric and statistical modeling with python. Proceedings of the 9th Python in Science Conference (SciPy 2010), 2010-06-28, Austin, Texas.

Sevanto S, Suni T, Pumpanen J, Grönholm T, Kolari P, Nikinmaa E, Hari P et Vesala T. 2006. Wintertime photosynthesis and water uptake in a boreal forest. Tree Physiology, 26 : 749-757.

Simard S, Morin H, Krause C, Buhay WM et Treydte K. 2012. Tree-ring widths and isotopes of artificially defoliated balsam firs: A simulation of spruce budworm outbreaks in Eastern Canada. Environmental and Experimental Botany, 81 : 44-54.

Société des établissements de plein air du Québec. 2024. Rapport annuel 2023-2024 de la Sépaq. Québec Sdédpad, Société des établissements de plein air du Québec, Québec, QC, 137 p.

Steppe K, Sterck F et Deslauriers A. 2015a. Diel growth dynamics in tree stems: linking anatomy and ecophysiology. Trends in Plant Science, 20 : 335-343.

Steppe K, von der Crone JS et De Pauw DJW. 2016. Treewatch.Net: A water and carbon monitoring and modeling network to assess instant tree hydraulics and carbon status. Frontiers in Plant Science, Volume 7 - 2016.

Steppe K, De Pauw DJW, Lemeur R et Vanrolleghem PA. 2006. A mathematical model linking tree sap flow dynamics to daily stem diameter fluctuations and radial stem growth. Tree Physiology, 26 : 257-273.

Steppe K, Vandegehuchte MW, Tognetti R et Mencuccini M. 2015b. Sap flow as a key trait in the understanding of plant hydraulic functioning. Tree Physiology, 35 : 341-345.

Tardif J, Flannigan M et Bergeron Y. 2001. An analysis of the daily radial activity of 7 boreal tree species, northwestern Quebec. Environmental Monitoring and Assessment, 67 : 141-160.

Turcotte A, Morin H, Krause C, Deslauriers A et Thibeault-Martel M. 2009. The timing of spring rehydration and its relation with the onset of wood formation in black spruce. Agricultural and Forest Meteorology, 149 : 1403-1409.

Van Rossum G et Drake FL. 2009. Python 3 reference manual. CreateSpace, Scotts Valley, CA, 242 p.

Virgin GVJ et MacLean DA. 2017. Five decades of balsam fir stand development after spruce budworm-related mortality. Forest Ecology and Management, 400 : 129-138.

Virtanen P, Gommers R, Oliphant TE, Haberland M, Reddy T, Cournapeau D, Burovski E, Peterson P, Weckesser W, Bright J, van der Walt SJ, Brett M, Wilson J, Millman KJ, Mayorov N, Nelson ARJ, Jones E, Kern R, Larson E, Carey CJ, Polat İ, Feng Y, Moore EW, VanderPlas J, Laxalde D, Perktold J, Cimrman R, Henriksen I, Quintero EA, Harris CR, Archibald AM, Ribeiro AH, Pedregosa F, van Mulbregt P, Vijaykumar A, Bardelli AP, Rothberg A, Hilboll A, Kloeckner A, Scopatz A, Lee A, Rokem A, Woods CN, Fulton C, Masson C, Häggström C, Fitzgerald C, Nicholson DA, Hagen DR, Pasechnik DV, Olivetti E, Martin E, Wieser E, Silva F, Lenders F, Wilhelm F, Young G, Price GA, Ingold G-L, Allen GE, Lee GR, Audren H, Probst I, Dietrich JP, Silterra J, Webber JT, Slavič J, Nothman J, Buchner J, Kulick J, Schönberger JL, de Miranda Cardoso JV, Reimer J, Harrington J, Rodríguez JLC, Nunez-Iglesias J, Kuczynski J, Tritz K, Thoma M, Newville M, Kümmerer M, Bolingbroke M, Tartre M, Pak M, Smith NJ, Nowaczyk N, Shebanov N, Pavlyk O, Brodtkorb PA, Lee P, McGibbon RT, Feldbauer R, Lewis S, Tygier S, Sievert S, Vigna S, Peterson S, More S, Pudlik T, Oshima T, Pingel TJ, Robitaille TP, Spura T, Jones TR, Cera T, Leslie T, Zito T, Krauss T, Upadhyay U, Halchenko YO, Vázquez-Baeza Y et SciPy C. 2020. SciPy 1.0: fundamental algorithms for scientific computing in Python. Nature Methods, 17 : 261-272.

Wilson KB, Hanson PJ, Mulholland PJ, Baldocchi DD et Wullschleger SD. 2001. A comparison of methods for determining forest evapotranspiration and its components: sap-flow, soil water budget, eddy covariance and catchment water balance. Agricultural and Forest Meteorology, 106 : 153-168.

Wu Y, MacLean DA, Hennigar C et Taylor AR. 2020. Interactions among defoliation level, species, and soil richness determine foliage production during and after simulated spruce budworm attack. Canadian Journal of Forest Research, 50 : 565-580.

Zhang Y, Xu G, Peng S, Bai J, Lu Q et Duan B. 2021. Water relations and non-structural carbohydrate responses to the combined effects of defoliation and progressive drought in a dioecious tree. New Forests, 52 : 605-619.

Zweifel R et Häsler R. 2000. Frost-induced reversible shrinkage of bark of mature subalpine conifers. Agricultural and Forest Meteorology, 102 : 213-222.

Zweifel R, Haeni M, Buchmann N et Eugster W. 2016. Are trees able to grow in periods of stem shrinkage? New Phytologist, 211 : 839-849.

Zweifel R, Sterck F, Braun S, Buchmann N, Eugster W, Gessler A, Häni M, Peters RL, Walthert L, Wilhelm M, Ziemińska K et Etzold S. 2021. Why trees grow at night. New Phytologist, 231 : 2174-2185.